

Avdelningen för Konstruktionsteknik  
Lunds Tekniska Högskola  
Box 118  
221 00 LUND

Division of Structural Engineering  
Faculty of Engineering, LTH  
P.O. Box 118  
S-221 00 LUND  
Sweden

## **Modelling Time-Dependent Effects for Segmentally Constructed Prestressed Concrete Bridges**

Modellering av tidsberoende effekter för etappvis utbyggda spännarmerade betongbroar

Joel Sunesson  
Niclas Elfving

2021

Rapport TVBK-5285  
ISSN 0349-4969  
ISRN: LUTVDG/TVBK-21/5285

Examensarbete  
Handledare: Jonas Niklewski (LTH), Christoffer Svedholm (ELU), Viktor Eriksson (ELU)  
Maj 2021

# Modelling Time-Dependent Effects for Segmentally Constructed Prestressed Concrete Bridges



Niclas Elfving  
Joel Sunesson  
V16

31st May 2021



# Abstract

Long-term effects, such as creep, shrinkage, and steel relaxation, are often difficult to predict for prestressed concrete structures. Creep as a phenomenon is complicated to describe and is therefore simplified in the current building standards, to better accommodate the designer. When dealing with segmentally constructed prestressed concrete bridges, these simplifications have shown to provide inaccurate predictions of the long-term effects. The aim of this Master's Thesis is to model these effects in a commercial Finite Element Analysis (FEA) program and to establish a reliable routine for future work in the area.

A thorough investigation of previous work were conducted regarding creep models and how they are implemented. The available methods in the program of choice were evaluated using a simple load case. A case study of the Jiang Jin Bridge, a prestressed concrete box girder bridge in Chongqing, China, was then performed. By implementing the chosen creep model in a long-term analysis for the case study the reliability of the model was increased.

Three creep models, time hardening, strain hardening, and a viscoelastic model, was compared to the current building code (Eurocode). The viscoelastic model was chosen to be the most appropriate, as it provided the most accurate results while also being easier to implement. By analysing the Jiang Jin Bridge with this model, it was shown that it could be used for larger and more complex structures.

The result of the case study strengthens the reliability of the viscoelastic creep model. Modelling the bridge with shell elements provided a more accurate description of the deflection history, compared to when beam elements were used. The behaviour cannot, however, be fully explained by using the creep model, and other time-dependant losses such as steel relaxation needs to be investigated further. A simplified calibration showed that the deflection history could be more accurately described by modifying the time-dependent losses for the post-tensioning tendons.

**Keywords**— Concrete, Creep, Segmentally constructed, Prestressing, Post-tensioning, Viscoelastic, Eurocode, Finite Element, Shell elements, Beam elements, Time-dependant, Steel relaxation



# Sammanfattning

Tidsberoende effekter, såsom krypning, krympning och stålrelaxation, är ofta svåra att prediktera när det kommer till förspända betongkonstruktioner. Krypning som ett fenomen är komplicerat och förenklas därför i gällande byggnormer (Eurocode), för att underlätta konstruktörens arbete. När det gäller etappvis spännarmerade betongbroar har dessa förenklingar visat sig ge felaktiga prognoser av de tidsberoende effekterna. Syftet med denna uppsats är att modellera dessa effekter i ett kommersiellt Finita Element program och därmed skapa en pålitlig rutin för framtida arbete inom området.

En djupgående undersökning gjordes kring olika krypmodeller och hur de kan implementeras. De tillgängliga metoderna i det valda programmet utvärderades med ett enkelt lastfall. En fallstudie av Jiang Jin Bridge, en etappvis spännarmerad betongbro i Chongqing, Kina, genomfördes sedan. Genom att implementera krypmodellen och analysera den valda bron över en tidsperiod på 10 år kunde modellens tillförlitlighet ökas.

Tre krypmodeller, tidshärdande, töjningshärdande och en viskoelastisk modell, jämfördes med hur krypning beaktas i den nuvarande byggnormen (Eurocode). Den viskoelastiska modellen valdes som den mest lämpliga, den gav de mest exakta resultaten samtidigt som den var lättare att implementera. Genom att analysera Jiang Jin Bridge med denna modell visades det att den kunde användas för större och mer komplexa konstruktioner.

Resultatet av fallstudien stärker tillförlitligheten hos den viskoelastiska krypmodellen. Modellering av bron med skalelement gav en mer exakt beskrivning av nedböjningshistoriken jämfört med när balkelement användes. Beteendet kan dock inte förklaras fullständigt med hjälp av krypmodellen och andra tidsberoende effekter såsom förluster i spännkablar behöver undersökas vidare. En förenklad kalibrering visade att nedböjningshistoriken kunde beskrivas mer exakt genom att ändra de tidsberoende förlusterna för de förspända spännkablarna.





# Acknowledgements

This Master's Thesis have been written at the division of Construction Science at the Faculty of Engineering, Lund University and in collaboration with ELU konsult Malmö. We would like to thank our supervisor at ELU, Christoffer Svedholm, and our supervisor from the faculty, Jonas Niklewski, who has given us continous support throughout the entire process. We would also like thank the ELU office in Malmö and the remaining professionals who have provided input on our work.

May 2021

Lund, Sweden

*Joel Sunesson and Niclas Elfving*



# Abbreviations

**EC** Eurocode

**FEA** Finite Element Analysis

**FEM** Finite Element Method



# List of Symbols

$\alpha$	Temperature coefficient associating the relative strain
$\alpha_1$	Coefficient considering concrete strength
$\alpha_2$	Coefficient considering concrete strength
$\alpha_3$	Coefficient considering concrete strength
$\beta(f_{cm})$	Factor on the notional creep coefficient to allow for concrete strength
$\beta(t_0)$	Factor on the notional creep coefficient to allow for age at loading
$\beta_{as}$	Time function of autogenous shrinkage strain
$\beta_c$	Time function of the creep coefficient
$\beta_{ds}$	Time function of drying shrinkage strain
$\beta_H$	Factor on $\beta_c$ to account for relative humidity and notional member size
$\chi_{1000}$	Stress relaxation after 1000 hours
$\chi$	Ageing coefficient
$\chi_\infty$	Stress relaxation factor after long time
$\chi_t$	Stress relaxation factor at time t
$\delta$	Vertical deflection [m]
$E$	Modulus of elasticity [Pa]
$E_0$	Modulus of elasticity at time $t_0$ [Pa]
$E_c$	Modulus of elasticity for concrete [Pa]
$E_{cm}$	Modulus of elasticity for concrete after 28 days [Pa]
$E_{c,eff}$	Effective modulus of elasticity for concrete [Pa]
$E_p$	Modulus of elasticity for prestressing steel [Pa]
$\epsilon_0$	Elastic strain
$\epsilon_c$	Total strain in concrete
$\epsilon_{c,creep}$	Strain in concrete due to creep
$\dot{\epsilon}^{cr}$	Strain in concrete due to creep, power law parameter
$\epsilon_{ca}$	Autogenous shrinkage strain
$\epsilon_{ca}(\infty)$	Final autogenous shrinkage strain
$\epsilon_{cd}$	Drying shrinkage strain
$\epsilon_{cd,0}$	Nominal unrestrained drying shrinkage
$\epsilon_{cd}(\infty)$	Final drying shrinkage strain
$\epsilon_{cs}$	Total shrinkage strain in concrete
$\epsilon_{pi}$	Initial strain of prestressing steel
$\epsilon_{p\infty}$	Total strain in prestressing steel after long time
$\epsilon^{vol}$	Total volumetric strain
$f_{ck}$	Characteristic strength for concrete [Pa]
$f_{cm,28d}$	Design strength for concrete after 28 days [Pa]
$f_{puk}$	Ultimate characteristic tensile strength of the prestressing steel [Pa]
$G_0$	Shear modulus at time $t = 0$ [Pa]
$g_R$	Dimensionless shear relaxation modulus
$G_R$	Shear relaxation modulus at time t [Pa]
$\gamma$	Total shear strain

$h_0$	Notional size of the concrete member [mm]
$J$	Total stress dependant strain from a constant applied stress
$j_K$	Normalized bulk compliance
$J_K$	Bulk compliance [1/Pa]
$j_S$	Normalized shear compliance
$J_S$	Shear compliance [1/Pa]
$k$	Wobble coefficient
$K_0$	Bulk modulus at time $t = 0$ [Pa]
$k_h$	Shrinkage coefficient depending on notional size, $h_0$
$k_R$	Normalized bulk modulus
$K_R$	Bulk modulus at time t [Pa]
$\mu$	Friction coefficient
$\nu$	Poisson's ratio
$\nu_0$	Poisson's ratio at time $t = 0$
$p_0$	Constant pressure [Pa]
$P_{max}$	Maximal force at stressing end in tendon [N]
$\Delta P_\mu(x)$	Loss in prestressing force due to friction located at distance x along the tendon [N]
$\varphi(\infty, t_0)$	Long term creep coefficient for concrete
$\varphi(t_c, t_0)$	Creep for coefficient for concrete at age $t_c$ where the structural system changes
$\varphi(t, t_0)$	Creep coefficient for concrete, loading at time $t_0$
$\varphi(t, t_i)$	Creep coefficient for concrete, loading at time $t_i$
$\varphi_0$	Notional creep coefficient for concrete
$\varphi_k(t, t_0)$	Creep coefficient for concrete at high stress levels
$\varphi_{RH}$	Factor on the notional creep coefficient to allow for relative humidity
$\tilde{q}$	Equivalent deviatoric stress [Pa]
$R$	Stress response from a constant applied strain
$RH$	Relative Humidity (%)
$s$	Coefficient describing the hardening rate of cement
$\mathbf{S}$	Deviatoric stress [Pa]
$S_0$	Internal actions from segmental construction sequence
$S_c$	Internal actions if the structure was to be cast in one
$\Delta S$	Redistribution of internal actions due to creep
$\sigma_0$	Stress in concrete applied at time $t_0$ [Pa]
$\sigma_c$	Stress in concrete at time t [Pa]
$\sigma_p$	Stress in prestressing tendons at time t [Pa]
$\sigma_{pi}$	Initial stress in prestressing tendons [Pa]
$\sigma_{psl}$	Loss in prestressing tendons due to anchorage slip [Pa]
$\sigma_{pmax}$	Maximal effective stress in prestressing tendon after tensioning [Pa]
$\Delta\sigma$	Stress difference [Pa]
$\Delta\sigma_\mu(x)$	Loss in prestressing tendons due to friction located at distance x along the tendon [Pa]
$\Delta\sigma_{pr}$	Stress loss in prestressing steel [Pa]
$t_0$	Time of loading (curing age) [days]
$T$	Temperature [ $^{\circ}C$ ]
$\tau_0$	Constant shear stress [Pa]
$\theta$	Rotational angle

# Contents

Abstract	I
Sammanfattning	III
Acknowledgements	V
Abbreviations	VII
List of Symbols	IX
Table of Contents	XIII
<b>1 Introduction</b>	<b>1</b>
1.1 Background . . . . .	1
1.2 Aim and Objectives . . . . .	1
1.3 Method and Research Questions . . . . .	2
1.4 Limitations . . . . .	2
<b>I Literature Study</b>	<b>3</b>
<b>2 History and Concept</b>	<b>5</b>
2.1 History of Prestressed Concrete . . . . .	5
2.1.1 Concept and Intuitive Designs . . . . .	5
2.1.2 Early Development . . . . .	5
2.1.3 Understanding of Time-Dependent Effects . . . . .	6
2.2 Case Study Concepts . . . . .	7
2.2.1 Cantilever Bridges . . . . .	7
2.2.2 Balanced Cantilever Method . . . . .	7
<b>3 Basic Theory</b>	<b>11</b>
3.1 Post-Tensioning . . . . .	11
3.1.1 Design of Post-Tensioning System . . . . .	12

XI

3.1.2	Installation of Post-Tensioning System . . . . .	13
3.1.3	Friction Losses . . . . .	15
3.2	Time-Dependent Effects . . . . .	16
3.2.1	Stress Relaxation of Steel . . . . .	16
3.2.2	Shrinkage . . . . .	19
3.2.3	Creep . . . . .	20
3.2.4	Time Hardening (Young’s Modulus) . . . . .	22
<b>4</b>	<b>Modelling of Creep</b>	<b>25</b>
4.1	Building Codes to Predict Creep . . . . .	25
4.2	Creep Models in Abaqus . . . . .	26
4.2.1	Time Hardening Model . . . . .	26
4.2.2	Strain Hardening Model . . . . .	30
4.2.3	Calibrating Time and Strain Hardening Parameters . . . . .	33
4.2.4	Viscoelastic Model . . . . .	34
4.2.5	Comparison of Creep Models . . . . .	36
4.3	Verification of Creep Models . . . . .	37
4.3.1	Time and Strain Hardening Model . . . . .	38
4.3.2	Viscoelastic Model . . . . .	39
4.3.3	Comparing Models when Unloading . . . . .	40
4.3.4	Development of Young’s Modulus . . . . .	40
4.3.5	Conclusion of Model best fit for Predicting Creep According to Eurocode	41
<b>II</b>	<b>Case Study</b>	<b>43</b>
<b>5</b>	<b>Jiang Jin Bridge Description</b>	<b>45</b>
5.1	Dimensions and Positioning of Tendons . . . . .	45
5.2	Properties . . . . .	47
5.3	Construction Sequence . . . . .	48
<b>6</b>	<b>Finite Element Model</b>	<b>51</b>
6.1	Modelling of Shrinkage . . . . .	52
6.2	Implementation of Creep in Abaqus . . . . .	52



6.3	Modelling of Tendons . . . . .	54
6.3.1	Losses due to Stress Relaxation . . . . .	54
6.3.2	Instantaneous Losses (Friction/Anchorage Slip) . . . . .	55
6.4	Modelling of the Construction Sequence . . . . .	57
<b>III</b>	<b>Results and Discussion</b>	<b>59</b>
<b>7</b>	<b>Case Study Analysis</b>	<b>61</b>
7.1	Deflections . . . . .	61
7.2	Analysis of Bending Moments . . . . .	66
7.2.1	Bending Moment due to Permanent Loads . . . . .	66
7.2.2	Influence of Tendons on the Bending Moment . . . . .	67
7.3	Calibration of Parameters . . . . .	68
7.4	Sources of Errors . . . . .	69
<b>8</b>	<b>Conclusions</b>	<b>73</b>
<b>9</b>	<b>Further Work</b>	<b>75</b>
	<b>Bibliography</b>	<b>77</b>



# 1 Introduction

## 1.1 Background

When designing prestressed concrete bridges, it is important to consider time-dependent effects such as creep, shrinkage, and steel relaxation. This is especially important when the bridge is cast and erected in several different stages, as this causes the structure to deform substantially and gradually during construction. A general problem with this construction method is that deformations induced by creep are difficult to accurately predict. There are numerous examples of bridges that have exhibited deformations larger than those predicted in design. One example is the Koror-Babeldaob bridge in Palau where the mid-span deflection was more than double that of what was predicted in the design stage (Bazant et al., 2012a).

The European building code, (Eurocode 2, 2005b), suggests four different methods for designing segmentally constructed concrete bridges with regards to creep:

1. General and incremental step-by-step method
2. Methods based on the theorems of linear viscoelasticity
3. The ageing coefficient method
4. Simplified ageing coefficient method

In the designers guide to Eurocode 2 (2005b), see Hendy and Smith (2007), only Method 1 and 4 are considered. Method 1 requires an iterative procedure whereas 4 can be performed using hand calculations. Furthermore, method 2 has been frequently used when more accurate modelling has been done for existing bridges, see for example (Canovic and Goncalves, 2005) and (Bazant et al., 2012b).

## 1.2 Aim and Objectives

Time-dependent effects for segmentally constructed concrete bridges are usually considered using simplified hand calculations, due to difficulties in describing time-dependent effects during the erection process. The overarching aim of this Master's Thesis is to evaluate the possibility of using numerical models to determine the long term behaviour of segmentally constructed prestressed bridges. By establishing a reliable routine, excessive long-term deformation can be avoided.

Different creep models were analysed for a simple load case to determine the one best suited. Existing measurements from a segmentally cast bridge were then used as a basis to further evaluate the performance of the chosen creep model.

## 1.3 Method and Research Questions

A literature study was initially carried out to address the following:

- What are the different mechanical and structural concepts involved in determining the long-term behaviour of prestressed segmentally constructed concrete bridges? What are the existing theories regarding creep, shrinkage, and prestressing losses?
- How can these effects be implemented numerically for segmentally constructed concrete bridges? What are the difficulties?

Numerical models (Brigade/PLUS, based on the Abaqus software) was then used to address the following:

- What are the available methods to model creep numerically? How, and under what circumstances, do they differ in their result?
- How can the creep models be verified by using a simple load case and comparing with the methods described in Eurocode (EC)?
- How can the global analysis be simplified to facilitate an efficient design process? Is it necessary to use shell elements or is it possible to model the bridge with beam elements?

A case study of the Jiang Jin Bridge was finally carried out using the acquired methods. The results were analysed with respect to long-term deformations and compared to measured values.

## 1.4 Limitations

The scope of this Master's Thesis is focused on long-term effects for bridges similar to the case study. The analysis is therefore limited to prestressed segmentally constructed concrete bridges with large spans. Due to the focus on long-term effects the study only considers permanent loads. It should be noted however, that depending on the frequency, traffic loads can induce cyclic creep (see for example Teng (2017)).

The analysis is limited to the FEA program of choice, the commercial software Brigade/PLUS. This means that the study will be somewhat limited to the chosen modelling program regarding the implementation of long-term effects. There will also be limitations regarding computational power and therefore simplifications must be made.

# Part I

## Literature Study



## 2 History and Concept

### 2.1 History of Prestressed Concrete

#### 2.1.1 Concept and Intuitive Designs

Prestressing as a concept has been used for a long time. Consider, for example, a classic English long bow. The weapon has a pretensioned string which is anchored by the opposite ends of a wooden strut. Another example are sailboats, where the mast is tied down and stiffened by pretensioned stays. The actual science behind prestressing, especially the long-term effects, were most likely not known at the time. Regardless, however, it is quite intuitive that the effect of prestressing will reduce over time and that retightening therefore is necessary. As described in Loewe and Llovera (2014), the understanding of these effects will be a key factor in the development of prestressed concrete. Figure 2.1 shows an example of an intuitive design using the concept of prestressing, in this case a timber bridge built in the early 19th century in Baltimore, United States. By loading the truss vertically, inserting secondary braces and then removing the load, the structure becomes fully compressed.

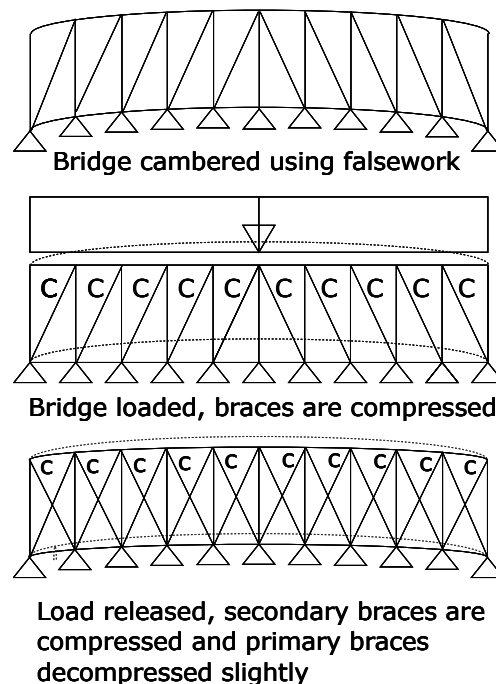


**Figure 2.1:** Prestressing principle of Long's Bridge (1829), recreated from Loewe and Llovera (2014).

#### 2.1.2 Early Development

In late 19th century numerous patents were obtained regarding the idea to prestress the steel in reinforced concrete. The American Peter Jackson, often considered as a pioneer in

prestressed concrete, received several patents between 1858 and 1888. The latter one included a way to handle bonding issues by installing metallic pieces at both ends and turnbuckles so that the steel chord could be retightened. These patents were then further developed by fellow countryman Thomas Lee, who also introduced high strength steel. Similar innovations were made in Europe during this period, for example Doerhing in 1888, although not as well recognised or documented. A common driver for prestressing at the time was improved fire resistance. For example, the tie rod in a masonry arch was believed to be better protected against fire if the structure was prestressed (Loewe and Llovera, 2014).

Following the advancements made by American engineers, several Europeans further developed the concept of prestressed concrete. The French engineer, Francois Chaudy, came up with an effective design of a post-tensioned concrete beam in 1894. The Norwegian Jens Lund obtained patents in 1907 regarding prestressed concrete slabs, building on the concepts from Jackson and Lee (Loewe and Llovera, 2014).

### 2.1.3 Understanding of Time-Dependent Effects

At the time when reinforced concrete became widely used the progress of prestressed concrete was still slow. One of the main reasons relate to the lack of high strength steel which reduces the losses due to steel relaxation and allows for a reduced cross-sectional area. Another reason is the lacking understanding of time-dependent effects, in particular those related to creep deformations.

The effects of shrinkage were known quite early. In 1908 the American Charles Steiner obtained a patent that compensated for the variations in concrete properties over time. The concept of prestressing concrete was not successful, however, until the 1930s when thorough studies were made regarding creep behaviour. Leading the development in this area was a French engineer, Eugène Freyssinet, who studied the subject for about three decades without proper recognition (Loewe and Llovera, 2014).

By this time high strength steel was also available. Combined with the understanding of shrinkage, creep, and steel relaxation the use of prestressed concrete grew substantially. In 1932 the German E. Hoyer started producing prestressed concrete elements, an idea later implemented by the Swedish company AB Strängbetong in the 1940s. Klockestrand bridge in Kramfors, was the first implementation of prestressed concrete in Sweden. It was built between 1938-1940 by Skånska Cementgjuteriet (now Skanska). Another famous example of early prestressed concrete structures are the concrete shells of the Sydney Opera House, designed by danish company Arup in the 1950s (Engström, 2011).



## 2.2 Case Study Concepts

### 2.2.1 Cantilever Bridges

The concept of the cantilever method in bridge construction predates prestressed concrete and can be traced back to the ancient bridges in China. The method was used to build bridges with larger spans to overcome natural obstacles like ravines or rivers. By using cantilever and transverse beams, they were able to build rigid supports that extends into the span, reducing the distance that had to be overcome through beam action (Dai et al., 2017). The two supports are then connected by placing a simply supported beam over the two supports, as seen in Figure 2.2.

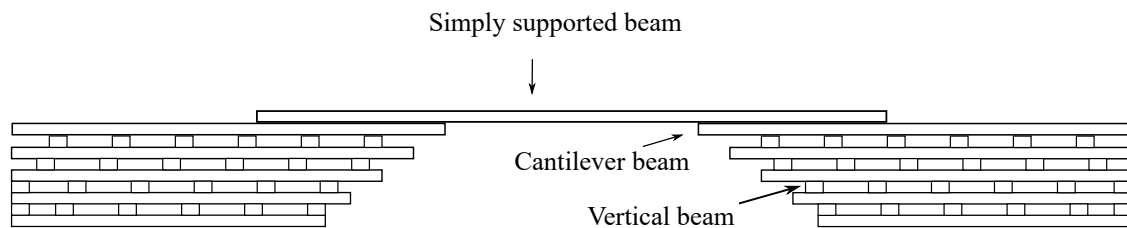


**Figure 2.2:** Example of an ancient Chinese bridge using the cantilever method, recreated from (Dai et al., 2017).

The first patent of a cantilever bridge was filed by Heinrich Gerber in 1866 (Mistewicz, 2015), who built the first modern bridge using the cantilever method (the Hussfurt Bridge over the Main River in Germany). The first modern cantilever bridges were built by using steel trusses, but prestressed concrete enabled the technique to be used with concrete. The first such bridge is usually attributed to the German engineer named Ulrich Finsterwalder (Billington et al., 2020), who developed a method to use concrete in cantilever bridges after the second world war. The method was first used during the construction of the Bendorf Bridge in 1962, spanning over the Rhine River at Koblenz in Germany.

### 2.2.2 Balanced Cantilever Method

The specific concept of a balanced cantilever construction is used in the case study and will be described in the following section. Figure 2.3 shows, conceptually, how a balanced cantilever bridge can be erected. Starting from the pylons, the superstructure is cast in segments. Each segment is balanced by a corresponding segment on the opposite side of the pylon. The segments can be cast-in-situ or precast and are tied to the previous segment by post-tensioning tendons and concreting. If the segments are precast, key segments are also used to ensure proper connection. The cycles are repeated until the superstructure from the two piers meet in the middle, after which the span is closed and post-tensioned in the bottom. The closure segments can be constructed as a rigid or hinged connection, (Lucko and Garza, 2003).

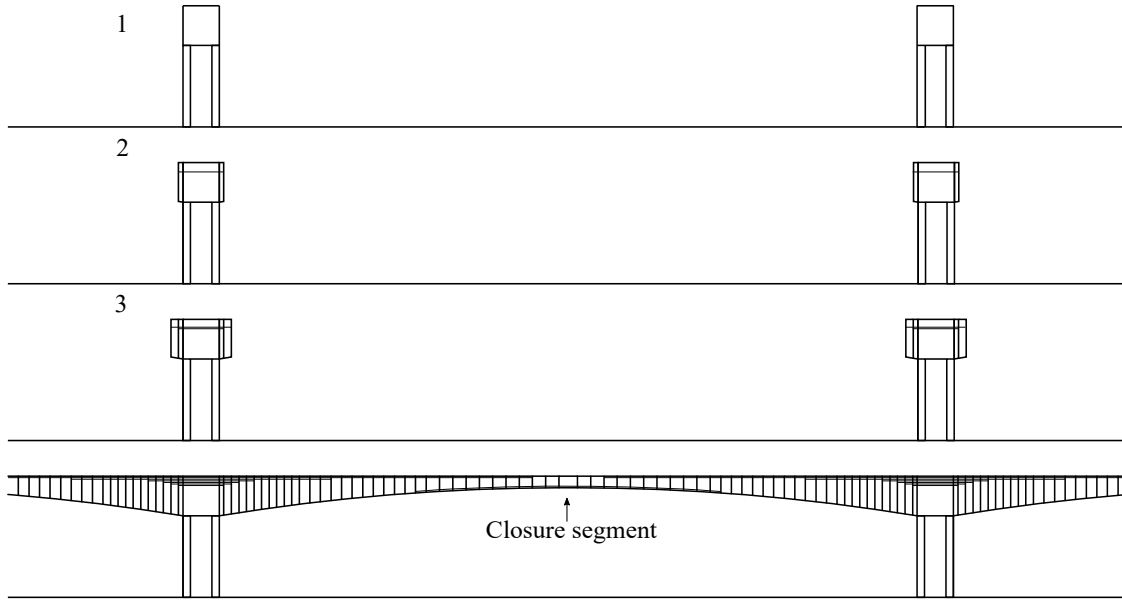


**Figure 2.3:** Example of bridge segmentally constructed using balanced cantilever method in, segments 1, 2, 3 and after last segments being completed.

If the spans are symmetrical, then no moment is imposed to the piers during the first phases (Kwak and Son, 2002). Prior to installing the closure segment, the structural system can be described by Figure 2.4a, where the moment over each pier due to a uniformly distributed load can be calculated as:

$$M = \frac{ql^2}{2} \quad (2.1)$$

Once the spans are closed, the structural state moves from cantilever state to a continuous beam over multiple supports, which leads to an elastic moment redistribution. In addition, time-dependent redistribution will also occur due to creep (Kwak and Son, 2002). If the span remains open the deflection  $\delta$  and rotational angle  $\theta$ , illustrated in Figure 2.4b, due to a uniformly distributed load can be calculated as:

$$\delta = \frac{ql^4}{8EI} \quad \text{and} \quad \theta = \frac{ql^3}{6EI} \quad (2.2)$$

where  $q$  is the uniformly distributed load,  $l$  the length from the support,  $E$  the elastic modulus and  $I$  the moment of inertia. If creep is considered, however, the deflection and rotation angle will increase over time according to:

$$\delta(t) = \delta_{t_0} \cdot (1 + \phi_t) \quad \text{and} \quad \theta(t) = \theta_{t_0} \cdot (1 + \phi_t) \quad (2.3)$$

where  $\delta_{t_0}$  and  $\theta_{t_0}$  are the elastic time-independent deflection and rotation angle calculated in equation (2.2),  $\phi_t$  is the creep factor at the time  $t$ . When the span is closed, the increase in rotation angle  $\theta \cdot \phi_t$  due to creep and additional loading is restrained. This restraint will lead to a moment in the span, effectively redistributing the moment over time as it increases in the span and decreases over the support.

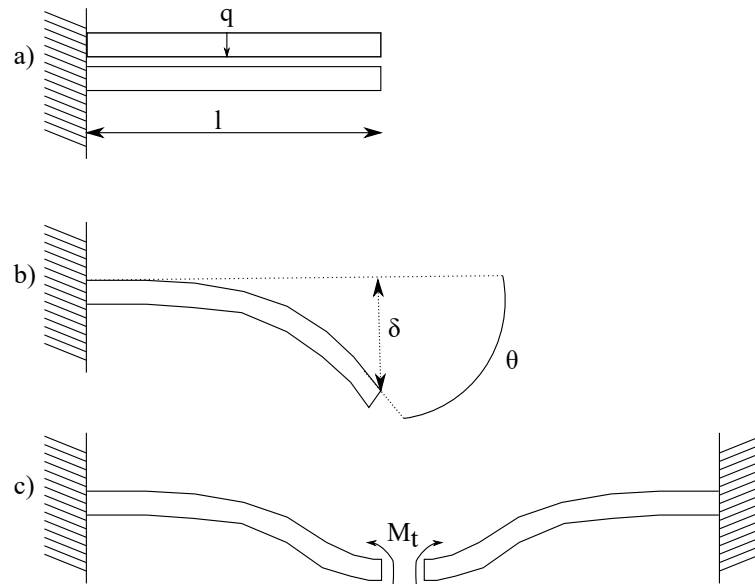


**Figure 2.4:** Figure demonstrating how the structural system and how it changes after the closure segment is installed, recreated from (Kwak and Son, 2002).

- a) The load case for the complete cantilever construction.
- b) The cantilever in its deformed state.
- c) The complete structure as the closure segment has been installed, the structural system has changed to a continuous beam.

By installing post-tensioning tendons to connect each segment during construction, a moment and compressive force is imposed to the system. This counteracts the bending moment which reduces the deflection  $\delta$  and rotational angle  $\theta$ . However, as the resulting force in the tendons decreases with time due to relaxation, shrinkage and creep, the counteracting effect will decrease.

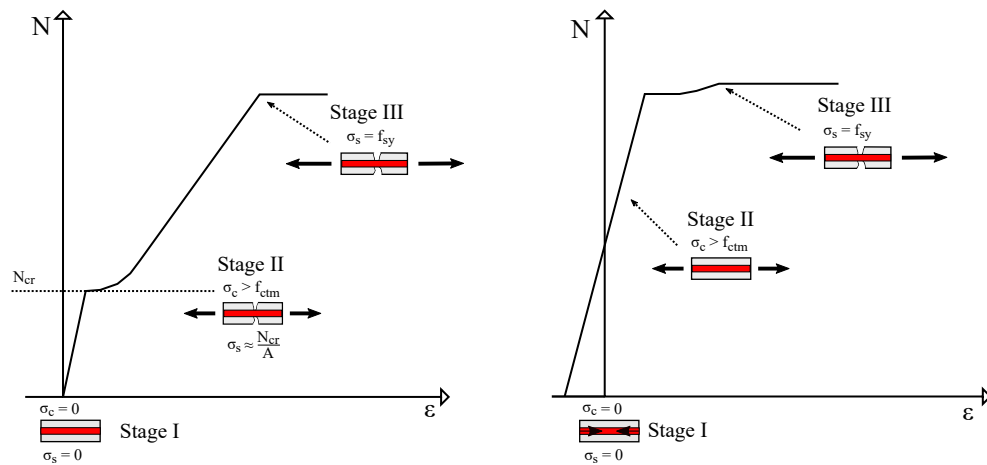


# 3 Basic Theory

## 3.1 Post-Tensioning

Reinforced concrete is cost effective and durable in a variety of applications and is therefore widely used. Concrete is normally reinforced by embedded steel to compensate for its poor tensile strength. The composite material works exceptionally well since concrete, if designed properly, is resistant to degradation while steel normally is not. When steel comes in contact with oxygen and water, corrosion will start to develop over time. Essentially the concrete cover protects the steel (Engström, 2011).

Figure 3.1 shows the behaviour of a concrete prism subjected to axial tensile force. Prior to cracking, the concrete and steel bars will interact to resist the load. At this point the area of both the steel and concrete will contribute to the stiffness, resulting in the initial slope according to Figure 3.1a (stage I). Once the concrete is fully cracked, the stiffness of the cross section is greatly reduced (see Figure 3.1a (stage II)). By prestressing, as seen in Figure 3.1b, an initial compression is induced to the concrete and cracks therefore develops at higher loads. This effectively reduces the deformations, while also protecting the embedded steel (Engström, 2011).

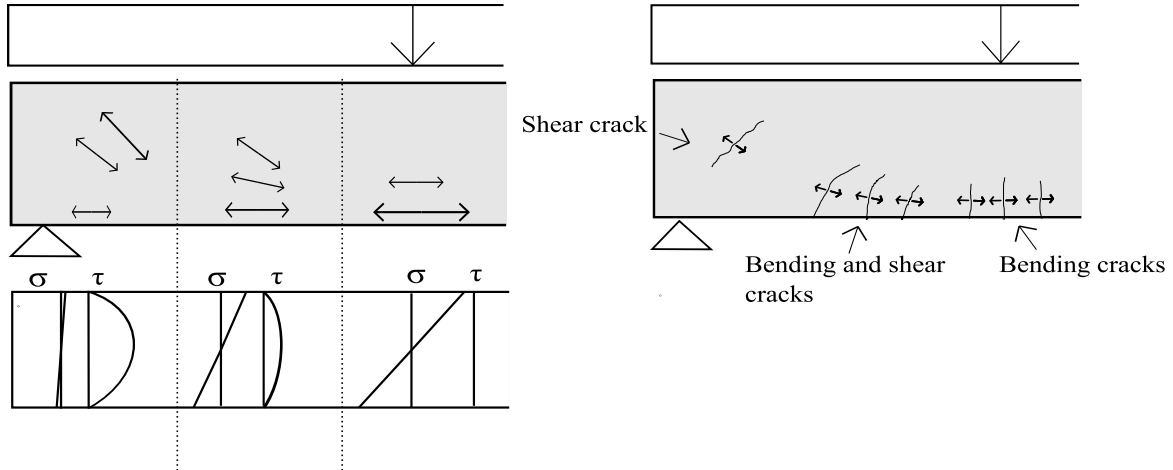


- (a) Normal reinforced beam.  
 Stage I, uncracked section (interaction between concrete and reinforcement).  
 Stage II, cracked section (The reinforcement takes all the load).  
 Stage III, cracked section (The steel is yielding).

- (b) Prestressed beam.  
 Stage I, uncracked section (interaction between concrete and reinforcement).  
 Stage II, same as stage I.  
 Stage III, cracked section (The steel is yielding).

**Figure 3.1:** Normal force - strain curve of a concrete prism subjected to tension. The difference between using normal reinforcement and prestressing is shown in three stages. Recreated from Engström (2011).

For a simply supported beam subjected to a vertical load, the internal forces and corresponding occurrence of cracks are shown in Figure 3.2. For structures that are not very sensitive to deflections and environmental effects, for example an indoor slab, this type of cracking is generally accepted. For concrete bridges, however, this is not desirable. Excessive deflections result in discomfort for users and the steel will be subjected to fast corrosion. Prestressing the concrete will limit the deflection and reduce the risk of both shear and bending cracks.



(a) Interaction of shear and tension, shown for different locations. (b) Occurrence of cracks due to these stresses.

**Figure 3.2:** Demonstrates the correlation between internal stresses and development of cracks, when a simply supported beam is subjected to a uniformly distributed vertical load. Recreated from Engström (2011).

Prestressing of concrete structures can be done either by pre-tensioning or post-tensioning. Pre-tensioning is done by applying a tensile force to the steel before casting and releasing once it has hardened. A typical example are the prefabricated HD/F elements that are widely used in the Swedish industry. Post-tensioning is done by tensioning the steel after the concrete has reached its intended strength. The concrete is then used as a support to the tensioning force that is successively increased (Engström, 2011). The following sections will describe the general theory of post-tensioning, which is the concept used for most concrete bridges and in the case study.

### 3.1.1 Design of Post-Tensioning System

The design of the prestressing system will have a considerable effect on how the structure behaves in service state. How large the prestressing effect will be is governed by the amplitude of the tensile force and the length of the lever arm to the centre of gravity,  $d_{ec}$ . These are chosen in design to meet desired performance of the structure. Figure 3.3 shows an example where a prestressing force results in a counteracting bending moment and compression, reducing the tension at the bottom part of the cross section.

When using a post-tensioning system, the vertical positioning of the tendons along the bridge can also be adapted to counteract the bending moment, illustrated in Figure 3.4 for a continuous beam over three supports. By designing the eccentricity of the tendons to follow the moment curve caused by permanent load, the moment is effectively counteracted. When the prestressing tendons are curved, however, friction and wobble will occur between

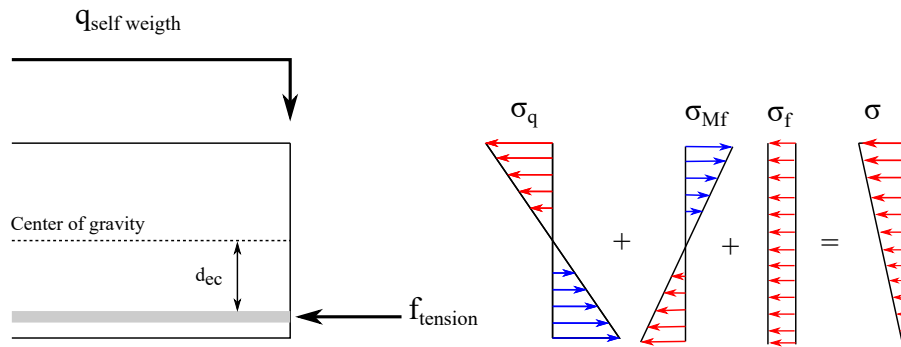


**Figure 3.3:** Stress acting in the cross-section, placed in the mid-span of simple supported post-tensioned concrete member.

the tendon and the duct which reduces the effective tensioning force. These losses will be discussed further in section 3.1.3.

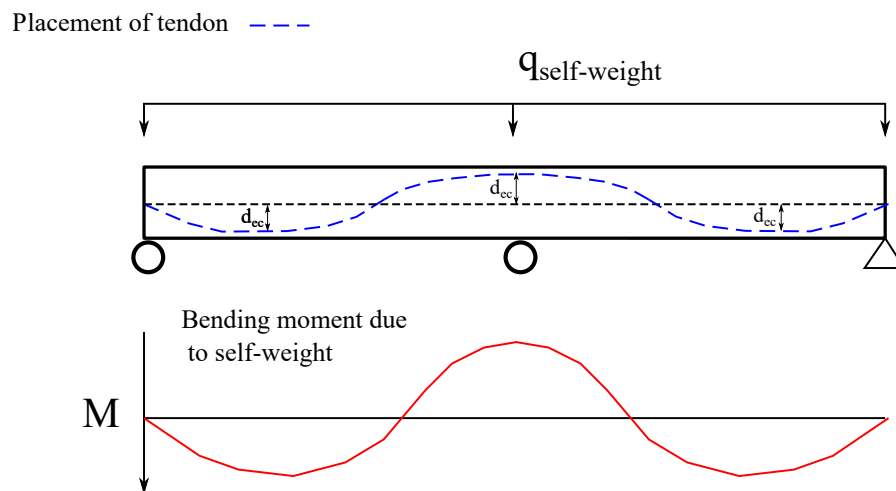


**Figure 3.4:** Placement of tendons in concrete member, adapted to counteract the bending moment caused by the self-weight.

### 3.1.2 Installation of Post-Tensioning System

The tendons may be manufactured on site or delivered prefabricated. To, for example, protect against corrosion, the tendons are placed inside a protecting duct. Figure 3.5 shows a duct with 19 tendons, each tendon consisting of seven strands where the outer strands are twisted around the middle strand. The ducts can be made of either plastic or steel and are placed in the structure to follow the desired curve. The tendons can be placed in the ducts before installation or pushed in once the ducts are in place (*European Technical Approval ETA-08/0012 Tensacciai Post-Tensioning Systems* 2017).

When the duct is positioned an anchorage is constructed at both ends. The stressing side typically has an anchorage as seen in Figure 3.6. On the dead end, the tendons are usually fixed by using a distance plate cast in the concrete. Reinforcement is also placed around the duct at the anchorage ends to ensure better force distribution to the concrete (*European Technical Approval ETA-08/0012 Tensacciai Post-Tensioning Systems* 2017).

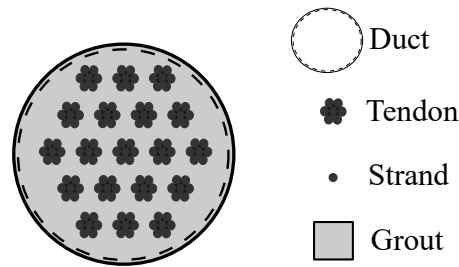


**Figure 3.5:** Typical profile of a duct with 19 tendons, each consisting of 7 strands, filled with grout.

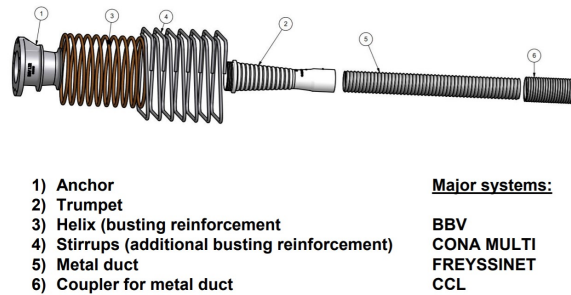


**Figure 3.6:** Typical design of an anchorage system, stressing side (Figure from BBV-systems, with permission).

The concrete of the structure is then cast, enfolding the ducts and the anchorage. Once the concrete has reached sufficient strength, normally 70 % of the 28 days design value (Engström, 2011), the tendons are tensioned by using a hydraulic jack. The tensioning can be done from either one or both sides. Once the tension force reaches the desired magnitude, the tendons are cut at the end/ends. By installing a cap with wedges at the end of the anchorage (see Figure 3.7), the contraction of the tendons is restrained. The force will, however, cause the wedges to draw into the anchorage, resulting in a small slip before completely locking in (Engström, 2011). The anchorage acts as support for the tendons, keeping them from going back to their previous length and distributing the force to the concrete. In this manner the tendons are kept in tension and a compressive force and moment are introduced to the structure, as seen in previous section and Figure 3.3.

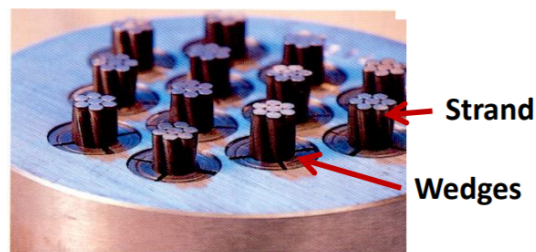


**Figure 3.7:** Illustrates a commonly used locking system at stressing side by using a wedge plate (Figure from BBV-systems, with permission).

Grout is then injected into the ducts to ensure proper connection between the tendons and the surrounding concrete, it also helps to protect the tendons from corrosion. The grout is injected through inlet holes that has been prepared at different location depending on the



length and placement of the duct. Outlet holes are normally placed at the highest points of the ducts, ensuring that no air gets trapped and that the duct gets completely filled with grout. Finally the protruding part of the tendons are cut and the cap is covered in a protecting layer of grout(Engström, 2011).

According to *European Technical Approval ETA-08/0012 Tensacciai Post-Tensioning Systems* (2017), the value of the anchorage slip should be chosen between 5-6 mm. The slip will cause the strain in the tendons to decrease, which leads to tension losses. The following equation can be used to calculate the loss of tension in the tendons due to slip,  $\sigma_{psl}$ .

$$\sigma_{psl} = \sigma_{pi} \cdot \frac{d_{slip}}{L_{tendon}} \quad (3.1)$$

where  $\sigma_{pi}$  is the initial stress,  $d_{slip}$  the distance slipped and  $L_{tendon}$  the length of the tendon.

### 3.1.3 Friction Losses

If the tendons have a curved profile, as seen in Figure 3.8, losses will occur due to friction between their surface and the duct. The duct will also have unintended deviations from the curvature, which increases the friction losses and is referred to as wobble. These deviations are due to the actual positioning of the ducts on site (Engström, 2011). A decrease in lever arm from  $d_{ec}$  to  $d_{ec,eff}$  can also be noted, due to the tendons pressing upwards against the top of the duct in the spans and downwards over the mid support. This effect can, however, often be neglected for large cross sections (as for the case study) and is therefore not accounted for here.

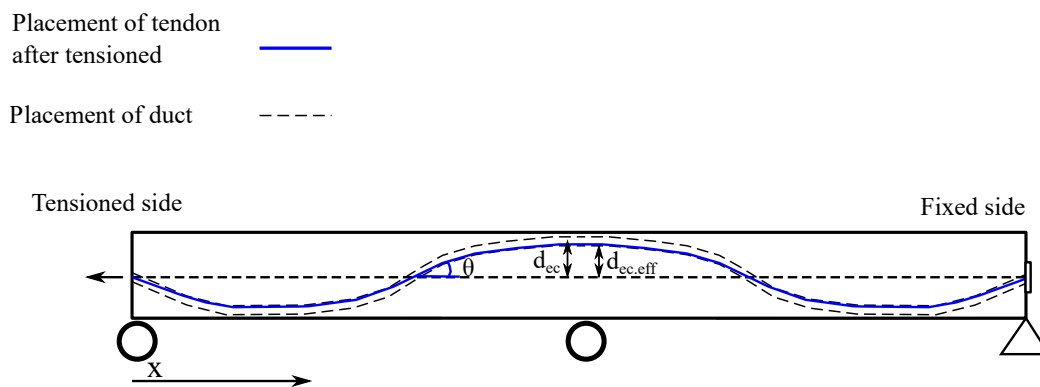


**Figure 3.8:** Placement and curvature of tendons after being tensioned.

An equation to calculate the loss in prestressing force due to friction located at distance  $x$  along the tendon,  $\Delta P_{\mu}(x)$ , is described in *European Technical Approval ETA-08/0012 Tensacciai Post-Tensioning Systems* (2017).

$$\Delta P_{\mu}(x) = P_{max}(1 - e^{-\mu(\theta+kx)}) \quad (3.2)$$

where  $\theta$  [rad] is the sum of the angular deviation from 0 up to  $x$  distance, irrespective of direction or sign.  $\mu$  is the frictional coefficient between the tendons and the ducts.  $P_{max}$  is the force at the stressing end.  $k$  [rad/m] is the non-intentional angular deviation inside tendons, also known as the wobble coefficient. Typical values of these coefficients are illustrated in Table 3.1.

**Table 3.1:** Values of friction and wobble coefficient, according to *European Technical Approval ETA-08/0012 Tensacciai Post-Tensioning Systems (2017)*.

System:	Internal	Internal	Internal	External
Duct material:	Steel	Plastic	Individually greased sheathed single strands	HDPE
Friction coef ( $\mu$ ):	0.16 - 0.24	0.12 - 0.14	0.05	0.1-0.12
Wobble coef ( $k$ ):	0.005 - 0.01	0.005 - 0.01	0.02 - 0.06	Neglected

According to Engström (2011), if the height of the cross-section is considerably smaller than the length of the span the distance  $x$  can be measured along the longitudinal axis instead as the arc length. Furthermore, the loss along the tendons can be assumed to vary linearly.

## 3.2 Time-Dependent Effects

### 3.2.1 Stress Relaxation of Steel

Stress relaxation is normally measured by applying a constant strain to a material and measuring the change in stress over time. Stress relaxation is thereby shown to be time-dependent, illustrated in Figure 3.9.

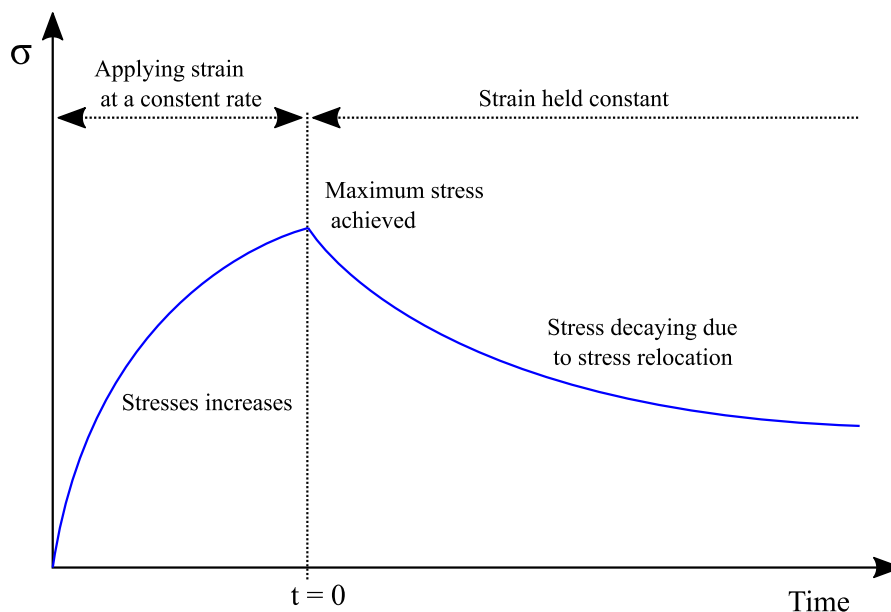


**Figure 3.9:** Typical illustration of stress relaxation by keeping a constant strain over time, recreated from (Ashter, 2018).

When subjected to stress, the microstructure of the steel will start to change over time. The grains will start to break which leads to cementite/ferrite lamellae and packets of dislocated debris beginning to form. Figure 3.10 shows the evolution of the microstructure during stress relaxation (note how the stress causes the cementite/ferrite lamellae to straighten out and even break at some points). The effect will cause the microstructure to align with the

direction of the stress, leading to permanent strains. The stress needed to keep the strain constant is thereby decreased. The permanent strain, which is caused by the stress relaxation, can be found by keeping the applied stress in the elastic region and then unloading. Figure 3.10 also indicates that the effect of stress relaxation also increases with the size of the initial stress. Greater initial stress leads to more expressed straightening and fracturing of the cementite/ferrite lamellae (Nguyen et al., 2020).

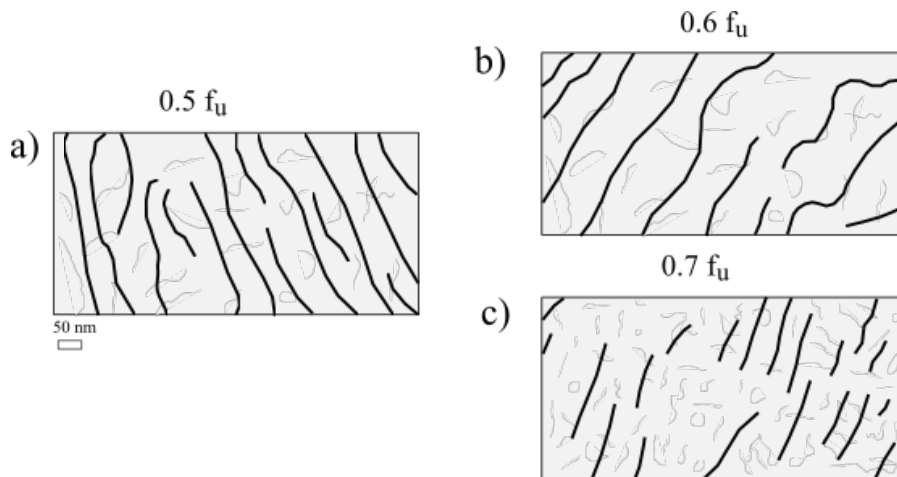


**Figure 3.10:** Dislocation of structure in steel specimens subjected to stress relaxation at different initial stresses, recreated from (Nguyen et al., 2020).

As explained by Engström (2011), the stress needed in the prestressing steel,  $\sigma_p$ , to keep a constant strain at time  $t$  is based on the initial stress,  $\sigma_{pi}$ , and can be determined as:

$$\sigma_p(t) = \sigma_{pi} - \chi_t \sigma_{pi} \quad (3.3)$$

where  $\chi_t$  is the relaxation factor at the given time  $t$ .

Furthermore, the relation in equation 3.3 can be used to find the effective modulus of elasticity as:

$$E_{p,ef} = E_p(1 - \chi_i) \quad (3.4)$$

However, both load and strain will vary with time in the prestressing steel. Even if the load were to be kept constant, the strain would still vary over time due to shrinkage and creep of the surrounding concrete. It is hard in practise to accurately determine steel stress at a given time. As such, approximate methods are generally used to account for the effects of stress relaxation. In Engström (2011), an approximate way to calculate the stress in the prestressing steel after long time is described as:

$$\sigma_{p\infty} = \epsilon_{p\infty} E_p - \chi_{\infty} \epsilon_{p\infty} E_p = \epsilon_{p\infty} E_p(1 - \chi_{\infty}) \quad (3.5)$$

The first term in equation 3.5 shows the elastic response at a given time. The second term illustrates the losses due to relaxation where the relaxation factor,  $\chi_{\infty}$ , is calculated based on the initial stress. This factor is both time and stress dependent, which is illustrated in Figure 3.9 and 3.10. As the maximum steel stress often equals the initial stress (due to e.g relaxation), the mean stress is generally lower than the initial. The relaxation factor used in equation 3.5 can therefore be seen as conservative. The final stress after long time, given by  $\epsilon_{p\infty}$  and  $E_p$ , is normally lower than the mean stress. By multiplying the conservative value,

$\chi_\infty$ , with the underestimated stress given by  $\epsilon_{p\infty}$  and  $E_p$  the two errors partly balance each other out.

A more accurate model to determine the steel relaxation is described in Eurocode 2 (2005a), which also consider the strain variation in the steel over time:

$$\sigma_p(t) = E_p \epsilon_{pi} (1 - 0.8 \chi_t) \quad (3.6)$$

where  $\epsilon_{pi}$  is the initial strain of prestressing steel and  $\chi_t$  is the relaxation factor at time  $t$ . The possibility to define the useful effective modulus of elasticity is, however, lost in equation 3.6.

The relaxation factor  $\chi_t$  is described in Eurocode 2 (2005a) as:

$$\chi_t = \frac{\Delta \sigma_{pr}}{\sigma_{pi}} \quad (3.7)$$

where  $\Delta \sigma_{pr}$  is the loss in stress due to relaxation and  $\sigma_{pi}$  the initial prestressing force. This relation at a certain time can be obtained by using test certificates from the manufacturer or alternatively be estimated from Eurocode 2 (2005a).

In EC, prestressing steel is divided into three relaxation classes, where the relaxation factor after 1000 hours,  $\chi_{1000}$ , is given in Table 3.2.

**Table 3.2:** Relaxation factor after 1000 hours according to Eurocode 2 (2005a).

Relaxation class	Prestressing steel	$\chi_{1000}$
1	Wire and strand with ordinary relaxation	0.08
2	Wire and strand with low relaxation	0.025
3	Hot-rolled and processed bars	0.04

Table 3.2 is based on tests performed with a constant temperature of  $20^\circ C$ , and with an initial stress of 70 % of the actual steel strength (Engström, 2011). According to the standard specification by ASTM International (2018) post-tensioning strands comprised of 7 individual wires should have a low relaxation class. This corresponds to relaxation class 2 according to Table 3.2.

The following equation is described in EC to calculate the relaxation factor for tendons of relaxation class 2:

$$\chi_t = 0.66 \cdot \chi_{1000} \cdot e^{9.1\mu} \cdot \left(\frac{t}{1000}\right)^{0.75(1-\mu)} \cdot 10^{-3} \quad (3.8)$$

where  $t$  is the time after tensioning in hours and  $\mu$  is given as:

$$\mu = \frac{\sigma_{pi}}{f_{puk}} \quad (3.9)$$

where  $f_{puk}$  is the ultimate characteristic tensile strength of the prestressing steel.

### 3.2.2 Shrinkage

As explained in Engström (2011) the total shrinkage ( $\epsilon_{cs}$ ) consists of two components: drying shrinkage,  $\epsilon_{cd}$ , and autogenous shrinkage,  $\epsilon_{ca}$ .

#### Autogenous shrinkage

Autogenous shrinkage, also called chemical shrinkage, is due to unhardened cement reacting with the remaining moisture inside the concrete. It reaches its long term value quickly compared to drying shrinkage and is described in Eurocode 2 (2005a) as:

$$\epsilon_{ca}(t) = \beta_{as}(t)\epsilon_{ca}(\infty) \quad (3.10)$$

where  $\beta_{as}(t)$  is the time function of autogenous shrinkage strain, calculated as:

$$\beta_{as}(t) = 1 - e^{-0.2t^{0.5}} \quad (3.11)$$

and  $\epsilon_{ca}(\infty)$  is the final autogenous shrinkage strain which increases linearly with higher concrete classes, calculated as:

$$\epsilon_{ca}(\infty) = 2.5(f_{ck} - 10)10^{-6} \quad (3.12)$$

#### Drying shrinkage

Drying shrinkage is due to moisture exchange between concrete and the surrounding environment. Compared to the autogenous shrinkage this process develops over a longer period. The magnitude of the final strain depends on the amount of water that is stored in the pores after casting the concrete. The rate depends largely on the relative humidity ( $RH$ ) of the surroundings and the area of the exposed surfaces relative to the thickness of the member (Engström, 2011). It is defined in Eurocode 2 (2005a) as:

$$\epsilon_{cd}(t) = \beta_{ds}(t)\epsilon_{cd}(\infty) \quad (3.13)$$

where  $\beta_{ds}(t)$  is the time function of autogenous shrinkage strain and  $\epsilon_{cd}(\infty)$  is the final drying shrinkage strain, which decreases with higher concrete classes. These parameters are described in the equations below:

$$\beta_{ds}(t) = \frac{t - t_0}{(t - t_0) + 0.04\sqrt{h_0^3}} \quad (3.14)$$

where  $t_0$  is the curing age (time at loading),  $h_0$  is the notional size of the element.

$$\epsilon_{cd}(\infty) = k_h\epsilon_{cd,0} \quad (3.15)$$

where  $k_h$  is a coefficient depending on the notional size,  $\epsilon_{cd,0}$  is the nominal unrestrained drying shrinkage.

### 3.2.3 Creep

In this section general equations to describe creep in all materials are first described. To capture the true behaviour, however, the mechanics of the specific material need to be studied in detail. Different theories to describe the different mechanical behaviours have been established. The behaviour of solid materials is especially complex due to many influencing factors (Betten, 2008). The most appropriate theories and equations used to simulate the behaviour of creep depends on the material being studied, the factors involved and their magnitude. Simplified methods according EC, commonly used to describe the creep of concrete, are finally shown.

#### General behavior of creep

Creep is a time and stress dependent strain that can be subdivided into Primary, Secondary and Tertiary creep, as seen in Figure 3.11. Temperature can be an important factor and is the main reason for tertiary creep. For concrete, however, tertiary creep is negligible in comparison to the other types and is therefore not further discussed.

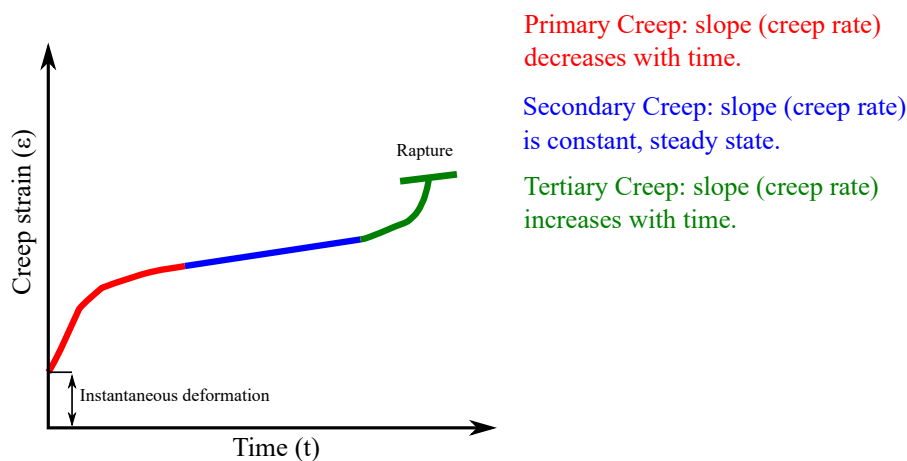


**Figure 3.11:** Illustrating the general behaviour of creep (material independent), divided into three stages to describe the creep rate, recreated from (Betten, 2008).

During the primary stage, the creep rate is controlled by the dislocations within the lattice structure, which starts to displace over time when stress is applied. The motion capacity of the present dislocations within the lattice will decrease as the deformation increases. This corresponds to strain hardening (see chapter 4.2.2). Continued deformation will result in new dislocations within the lattice which leads to higher dislocation density (Günther and Salzer, 2012). Higher dislocation density means that more energy is needed to maintain the current deformation rate and if the energy added by applying a stress is not increased the rate will decrease. Higher dislocation density also means that the current energy in the structure will be divided by a higher mass and therefore lower energy for each dislocation. This will lead to some dislocations being recovered. This is called relaxation of the material. When balance between relaxation and strain hardening has been achieved, the strain rate will be constant and enter the secondary creep stage.

A general equation is used to capture the instant strain of a body being subjected to the stress  $\sigma_0$ , by dividing the strain into elastic and plastic strain:

$$\epsilon_0 = \frac{\sigma_0}{E(T)} + \epsilon_p(\sigma_0, T) \quad (3.16)$$

where  $T$  is the temperature and  $E$  is the elastic modulus. However, to calculate creep, time is also an important factor. A simplified equation has been established to capture the creep strain in Figure 3.11, (Betten, 2008).

$$\epsilon_{cr} = \epsilon(t) - \epsilon_0 \propto t^\kappa \quad (3.17)$$

where  $\kappa < 1$  represent the primary,  $\kappa = 1$  the secondary and  $\kappa > 1$  the tertiary creep stages.

Due to the creep rate being constant during the secondary stage and tertiary creep not being relevant, it is mainly the primary creep behaviour that is of interest. The primary creep will also govern the magnitude of the final creep.

## Creep for concrete

Apart from deforming elastically when stressed, concrete will be subjected to creep deformation. The creep strain,  $\epsilon_{c,creep}$ , increases with the concrete stress,  $\sigma_c$ , and is defined in Eurocode 2 (2005a) as:

$$\epsilon_{c,creep}(t) = \varphi(t, t_0) \frac{\sigma_c}{E_c} \quad (3.18)$$

where  $\varphi(t, t_0)$  is the creep function depending on time ( $t$ ) and time of loading ( $t_0$ ),  $E_c$  is the elastic modular ratio for concrete. The magnitude of the creep function depends largely on the age of the concrete when the structure is loaded ( $t_0$ ) and is determined by:

$$\varphi(t, t_0) = \beta_c(t, t_0) \varphi_0 \quad (3.19)$$

where  $\beta_c(t, t_0)$  determines how the creep function varies with time and  $\varphi_0$  is the notional creep coefficient, calculated as:

$$\beta_c(t, t_0) = \left[ \frac{(t - t_0)}{(\beta_H + t - t_0)} \right]^{0.3} \quad \text{and} \quad \varphi_0 = \varphi_{RH} \cdot \beta(f_{cm}) \cdot \beta(t_0) \quad (3.20)$$

where  $\beta_H$ , in the left expression, is a factor that depends on the relative humidity and the notional member size. In the right expression,  $\varphi_{RH}$  accounts for the relative humidity,  $\beta(f_{cm})$  for the concrete strength, and  $\beta(t_0)$  for the time of loading. These parameters are described further in section 6.2.

An important note is that the above relations apply as long as the compression in the concrete does not exceeds  $0.45f_{ck}$  ( $f_{ck}$  is the characteristic compressive strength of concrete). In general the long-term compressive stresses should be kept below this value. If this stress is exceeded  $\varphi(t, t_0)$  is replaced with  $\varphi_k(t, t_0)$ .

Figure 3.12 illustrates, conceptually, the creep function due to a load applied at time  $t_0$ . Similarities can be found with the primary and secondary creep curve from Figure 3.11.

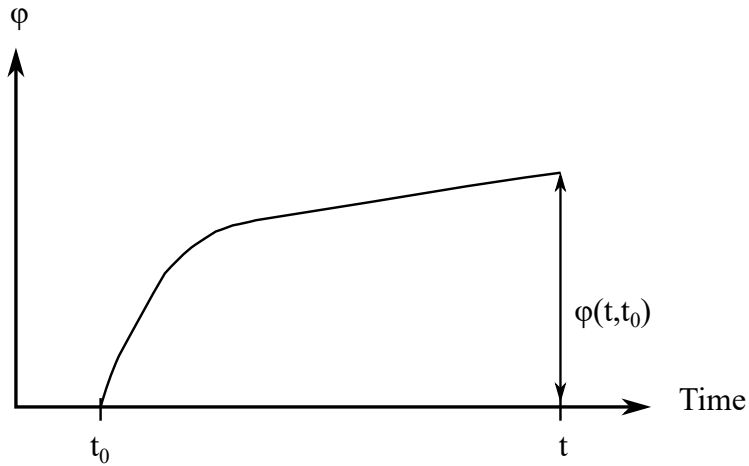


**Figure 3.12:** Illustrating the general behaviour of creep in concrete using the creep function described in EC.

### 3.2.4 Time Hardening (Young's Modulus)

Time hardening is a process where the material gains strength over time. Examples of properties affected by time includes hardening of concrete and the development of Young's Modulus (see Figure 3.13). Once water is added the cement will start to hydrate, effectively increasing the stiffness of the material over time (Council et al., 1997). In practise, the design value of the Young's Modulus is usually based on the stiffness after 28 days.

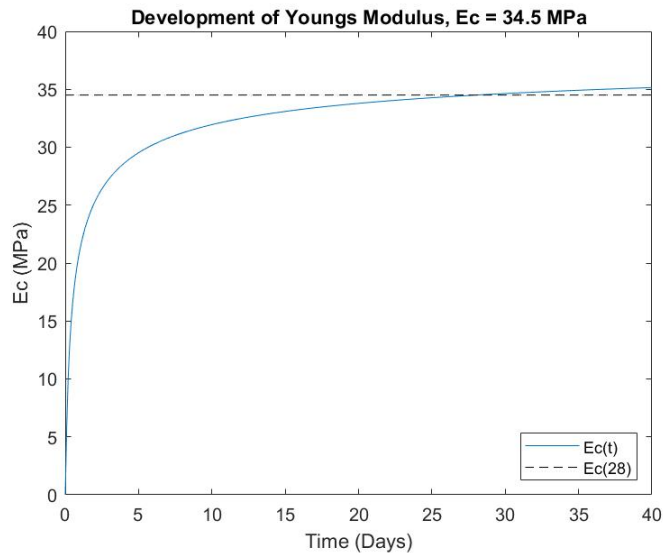


**Figure 3.13:** Development of Young's Modulus for concrete, based on EC (Cement class R).

The value of Young's Modulus over time is calculated by multiplying the mean elastic modular ratio,  $E_{cm}$ , with a time function described in Eurocode 2 (2005a) as:

$$E_c(t) = \beta_E(t)E_{cm} \quad (3.21)$$

where the time function  $\beta_E(t)$  can be calculated as:



$$\beta_E(t) = (\beta_{cc}(t))^{0.3} \quad (3.22)$$

and

$$\beta_{cc}(t) = e^{s - (1 - (\frac{28}{t})^{0.5})} \quad (3.23)$$

where  $t$  is the age of the concrete in days and  $s$  is a coefficient depending on the choice of cement (see Table 3.3).

**Table 3.3:** Hardening rate for different cement classes according to Eurocode 2 (2005a).

	Class R	Class N	Class S
s	0,20	0,25	0,38



# 4 Modelling of Creep

## 4.1 Building Codes to Predict Creep

The influence of creep in concrete is described in section 3.2.3. With varying long-term loads, such as in the case of segmentally constructed bridges, the behaviour becomes more complicated. This report will be limited to the methods described in Eurocode 2 (2005b), it should be noted that there are several other methods available.

### 1. General and incremental step-by-step method

- This method requires the designer to carry out structural analysis at several steps. The fundamental equation for time-dependent concrete strain is written as:

$$\epsilon_c(t) = \frac{\sigma_0}{E_c(t_0)} + \varphi(t, t_0) \frac{\sigma_0}{E_c(28)} + \sum \left( \frac{1}{E_c(t_i)} + \frac{\varphi(t, t_i)}{E_c(28)} \right) \Delta\sigma(t_i) + \epsilon_{cs}(t, t_s) \quad (4.1)$$

where the first term represents the instant deformation from a stress applied at time  $t_0$ , the second term represents the corresponding creep, the third term corresponds to the instant and creep deformation occurring due to variations in stress, and the fourth term describes the deformation due to shrinkage.

### 2. Methods based on the theorems of linear viscoelasticity

- The time-dependent properties of concrete can be described by:
  - $J(t, t_0)$  which represents the strain response at time "t" resulting from a constant applied stress at time " $t_0$ ".
  - $R(t, t_0)$  which represents the stress response at time "t" from a constant applied strain at time " $t_0$ ".

### 3. The ageing coefficient method

- This method allows for an analysis to be performed without having to take the discrete time steps into account. It is based on the ageing coefficient,  $\chi$ , and is useful when only the long term effects are of interest (Eurocode 2, 2005b).

### 4. Simplified ageing coefficient method

- The principle of this simplified method is to first calculate the internal forces of the structure by modelling the complete construction sequence, and then repeating the calculations assuming the structure was cast-in-one. By interpolating between these two cases the redistribution due to creep can be found as:

$$\Delta S = (S_c - S_0) \frac{\varphi(\infty, t_0) - \varphi(t_c, t_0)}{1 + \chi\varphi(\infty, t_0)} \quad (4.2)$$

where  $S_c$  are the internal actions from the segmental construction sequence,  $S_0$  are the internal actions if the structure was to be cast in one go. According to Hendy and Smith (2007) the factor  $\frac{\varphi(\infty, t_0) - \varphi(t_c, t_0)}{1 + \chi\varphi(\infty, t_0)}$  typically has as value between 0.65 and 0.8.

## 4.2 Creep Models in Abaqus

The material properties in Abaqus need to be adjusted to perform a creep analysis. There are several ways to do this, see Simulia (2014), but in this report the following models are investigated:

- Function \*CREEP and the subfunctions time/strain hardening.
- Function \*VISCOELASTIC in the time domain where the losses are caused by the internal damping effect of the material. This corresponds to the method described in section 4.1 (Methods based on the theorems of linear viscoelasticity).

### 4.2.1 Time Hardening Model

As previously illustrated in section 3.2.4, concrete has time hardening properties. This indicates that a time hardening model could be a good choice when calculating the creep strain. If the structure is loaded at different times, Young's Modulus will have different values, as shown in Figure 4.1. This will then also affect the magnitude of the creep strain.

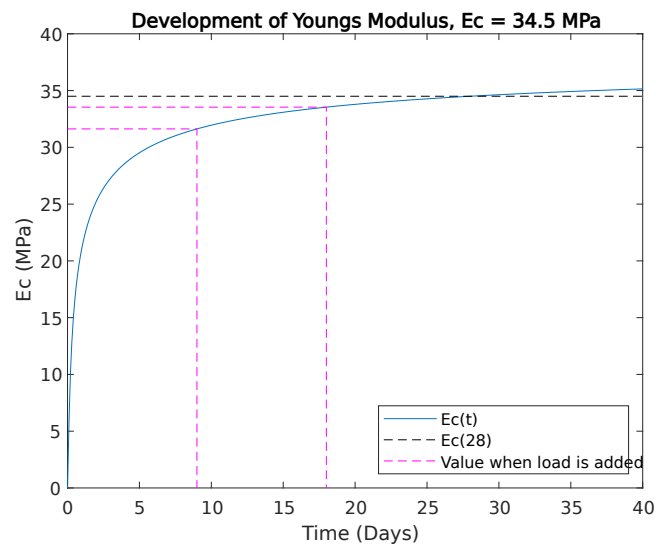


**Figure 4.1:** Difference in Young's Modulus when loaded at different times during hardening.

### Time hardening model in Abaqus

Time hardening uses a power law model where the creep strain rate is time-dependent, and the material stiffness increases over time. When load is added at a given time, the creep strain rate will increase to the rate obtained by the sum of the loads, as shown in Figure 4.2.

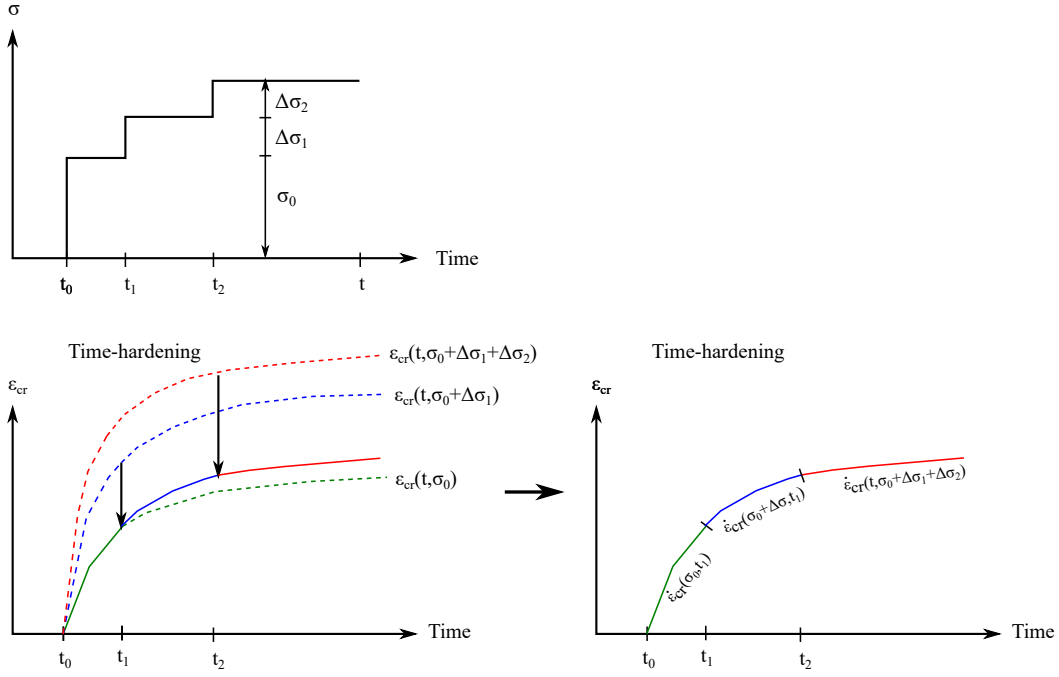


**Figure 4.2:** Left figure shows how the creep strain rate changes when load is added, based on time hardening theory. Right figure shows the resulting accumulated creep strain.

The equation used to calculate the creep strain rate in the Abaqus manual (Simulia, 2014) is given as:

$$\dot{\epsilon}^{cr} = A\tilde{q}^n t^m \quad (4.3)$$

where  $\dot{\epsilon}^{cr}$  is the uniaxial equivalent creep strain rate defined as:

$$\dot{\epsilon}^{cr} = \sqrt{\frac{2}{3} \dot{\epsilon}^{cr} : \dot{\epsilon}^{cr}} \quad (4.4)$$

$\tilde{q}$  is the uniaxial equivalent deviatoric stress according to Von Mises if the creep behaviour is isotropic or Hill's if anisotropic. For von mises,  $\tilde{q}$  is calculated as:

$$\tilde{q} = \sqrt{\frac{2}{3} \mathbf{S} : \mathbf{S}} \quad (4.5)$$

where  $\mathbf{S}$  is the deviatoric stress.

$A$ ,  $n$  and  $m$  are temperature dependant parameters which are determined experimentally,  $A$  and  $n$  needs to be positive and  $-1 < m < 0$ .

The equation used in Abaqus is based on the creep strain equation by Bailey and Norton (Betten, 2008).

$$\epsilon_{cr} = A\sigma^n t^m \quad (4.6)$$

where time and stress are variables, which characterises the time hardening theory. The derivative with regards to time can be expressed as:

$$\dot{\epsilon}_{cr} = Am\sigma^n t^{m-1} \quad (4.7)$$

However, Abaqus refers to the uniaxial equivalent creep strain and equivalent deviatoric stress. The equation developed by Bailey and Norton is also based on uniaxial stress but not the equivalent and only calculates the strain in one direction. For the one dimensional case with an isotropic material, the equivalent uniaxial creep strain rate and stress are equal to the uniaxial creep strain rate and stress ( $\dot{\bar{\epsilon}}^{cr} = \dot{\epsilon}^{cr}$  and  $\bar{q} = \sigma$ ). If the material is anisotropic the relation between the strains in the different directions need to be established before changing the variables (Simulia, 2014).

Several variations of the Bailey and Norton equation can be found in the literature, which leads to different material parameters. The parameters that are to be used needs to be specifically determined to fit the model in Abaqus. One way to determine the parameters is to perform tests on the material, which will be a time-consuming process. It's easier to look at tests already performed or to calibrate them against EC, the latter is chosen in this report.

To calibrate the parameters the creep strain is required. The creep strain is derived by integrating equation 4.3 with respect to time, stress is independent of time in this regard.

$$\bar{\epsilon}^{cr} = A\bar{q} \frac{t^{m+1}}{m+1} + C \quad (4.8)$$

where  $C$  is a constant which corresponds to the elastic strain,  $\epsilon_0$ . By replacing the equivalent strain and deviatoric stress with the uniaxial for an isotropic material, the following equation is obtained:

$$\epsilon^{cr} = A\sigma^n \frac{t^{m+1}}{m+1} + \epsilon_0 \quad (4.9)$$

For a one-dimensional case, the creep law can be integrated directly to find the solution. In other cases, numerical methods must be used where the time is divided into time steps in which iterations are performed until equilibrium is reached.

## Referring to EC

The parameters can be decided by referring to EC and the creep function,  $\varphi(t, t_0)$ , see section 3.2.3. The time hardening theory indicates that the creep function is established solely based on the concrete age when the first load is applied. If further loads are added, the additional creep will be based on the creep function caused by the initial load, resulting in a creep rate according to Figure 4.2. This method will underestimate deformations, as loads added after some time will result in little or no creep.

The behaviour of the time hardening model, and how the total strains can be calculated using the creep function, is shown in Figure 4.3 and the following relations.

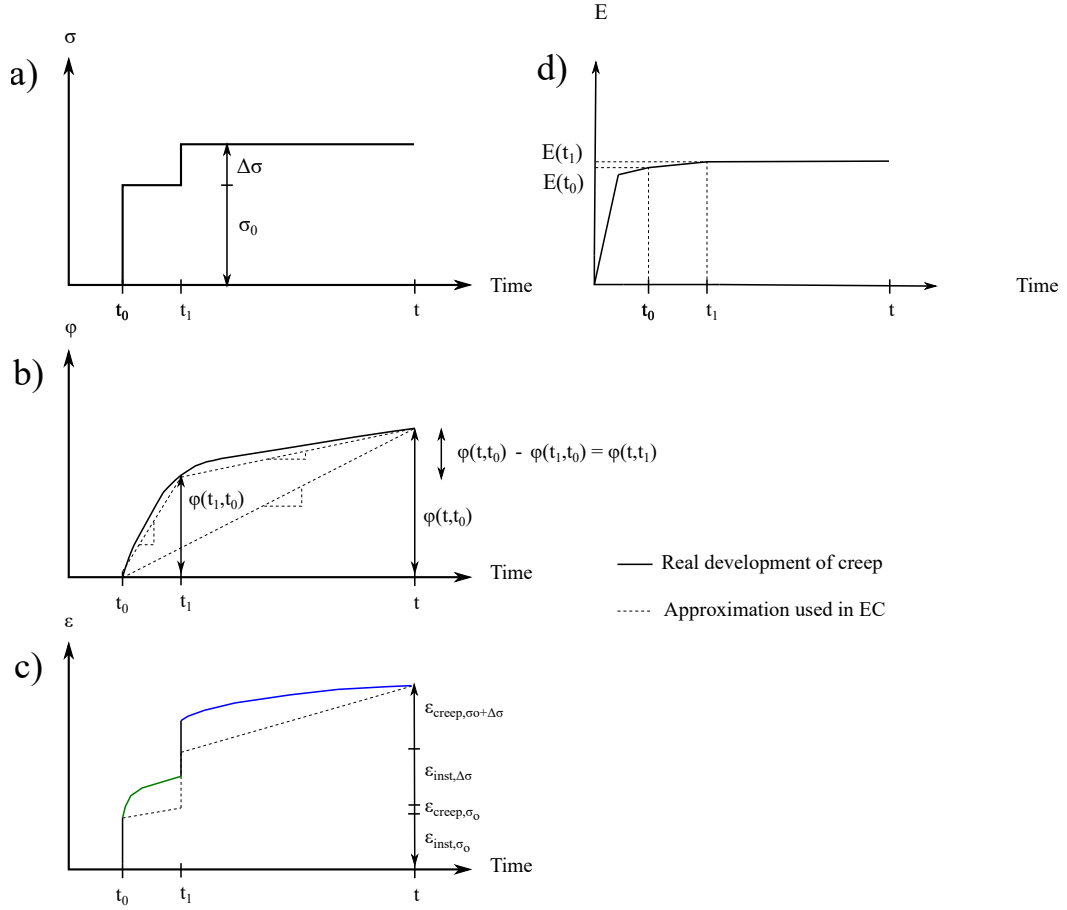


**Figure 4.3:** Showing how the stress (a), creep coefficient (b), total strain (c) and Young's Modulus (d) varies over time, based on time hardening theory.

$$\begin{aligned}
 \epsilon_{inst,\sigma_0} &= \frac{\sigma_0}{E(t_0)} \\
 \epsilon_{creep,\sigma_0} &= \frac{\sigma_0}{E(t)} \varphi(t_1, t_0) \\
 \epsilon_{inst,\Delta\sigma} &= \frac{\Delta\sigma}{E(t_1)} \\
 \epsilon_{creep,\sigma_0+\Delta\sigma} &= \left( \frac{\sigma_0}{E(t_0)} + \frac{\Delta\sigma}{E(t_1)} \right) (\varphi(t, t_0) - \varphi(t_1, t_0))
 \end{aligned} \tag{4.10}$$

where the creep strain follows the conceptual curve from Figure 4.2. The following equation for the total strain is achieved:

$$\epsilon(t) = \frac{\sigma_0}{E(t_0)} [1 + \varphi(t, t_0)] + \sum_{i=1}^n \frac{\Delta\sigma_i}{E(t_i)} [1 + \varphi(t, t_0) - \varphi(t_i, t_0)] \tag{4.11}$$

Which is similar to the equation described in section 4.1 (General and incremental step-by-step method). However, the equation above is using the initial creep function for all loads instead of a unique function based on the age of the concrete when each load is applied.

## 4.2.2 Strain Hardening Model

Strain hardening is mainly used to describe materials where creep occurs as the material undergoes plastic deformations. Concrete shows strain hardening properties when loaded in its plastic range by compression, as shown in Figure 4.4. Using a strain hardening model could therefore give a good estimation of the creep strain if the concrete were to be stressed in the plastic range. However, concrete also undergoes creep deformation in the elastic range, indicating that this model provides inaccurate results.

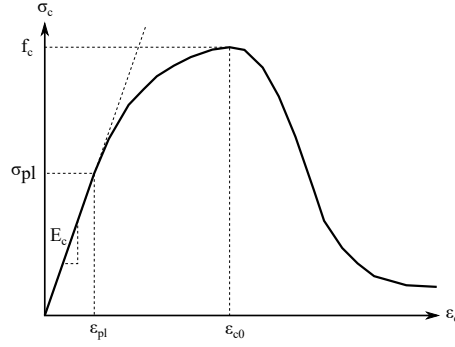


**Figure 4.4:** Typical stress-strain curve for concrete in compression, recreated from (Engström, 2008).

### Strain hardening model in Abaqus

Strain hardening also uses a power law model to describe the creep rate. For strain hardening, however, the creep rate is calculated based on the current creep strain and will be time-independent. When loads are added, the creep strain rate changes according to the rate of the sum of the loads with the current strain, as seen in Figure 4.5.

In the Abaqus manual (Simulia, 2014), the creep rate is calculated as:

$$\dot{\epsilon}^{cr} = (A\tilde{q}^n[(m+1)\bar{\epsilon}^{cr}]^m)^{\frac{1}{1+m}} \quad (4.12)$$

where the parameters and variables are the same as for time hardening, see previous section. This equation can be derived by first looking at the Bailey and Norton equation.

$$\epsilon_{cr} = A\sigma^n t^m \quad (4.13)$$

The derivative is the same as for time hardening:

$$\dot{\epsilon}_{cr} = Am\sigma^n t^{m-1} \quad (4.14)$$

The time, however, need to be replaced by the strain hardening factor. The strain hardening factor can be found by extracting the time from equation 4.13.

$$\epsilon_{cr} = A\sigma^n t^m \Rightarrow t = (\epsilon_{cr} A^{-1} \sigma^{-n})^{\frac{1}{m}} \Rightarrow t^{m-1} = (\epsilon_{cr} A^{-1} \sigma^{-n})^{1-\frac{1}{m}} \quad (4.15)$$



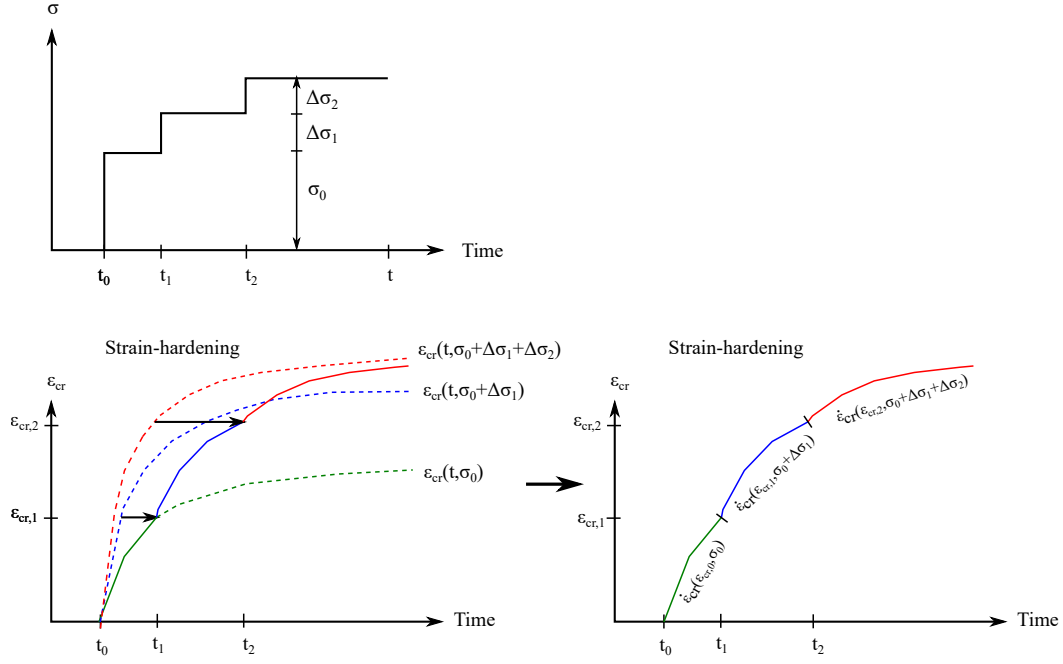


**Figure 4.5:** Left figure shows how the creep strain rate changes when load is added, based on strain hardening theory. Right figure shows the resulting accumulated creep strain.

The time in the derived expression, equation 4.14, is then replaced with the strain hardening factor:

$$\dot{\epsilon}_{cr} = Am\sigma^n t^{m-1} \Rightarrow \dot{\epsilon}_{cr} = Am\sigma^n (\epsilon_{cr} A^{-1} \sigma^{-n})^{1-\frac{1}{m}} \Rightarrow \dot{\epsilon}_{cr} = mA^{\frac{1}{m}} \sigma^{\frac{n}{m}} \epsilon_{cr}^{\frac{m-1}{m}} \quad (4.16)$$

The equation Abaqus uses as strain hardening can then be derived in the same way as described for Bailey and Norton. First, equation 4.3 is integrated with respect to time to obtain the creep strain.

$$\bar{\epsilon}^{cr} = \int A\bar{q}^n t^m dt = \frac{A\bar{q}^n t^{m+1}}{m+1} \quad (4.17)$$

The strain hardening factor is then obtained in the same way as described previously, for Bailey and Norton equation 4.15, as:

$$\begin{aligned} t &= (\bar{\epsilon}^{cr} (m+1) A^{-1} \bar{q}^{-n})^{\frac{1}{m+1}} \Rightarrow t^m = (\bar{\epsilon}^{cr} (m+1))^{\frac{m}{m+1}} (A^{-1} \bar{q}^{-n})^{1-\frac{1}{m+1}} \\ &= (\bar{\epsilon}^{cr} (m+1))^{\frac{m}{m+1}} (A\bar{q}^n)^{-1} (A\bar{q})^{\frac{1}{m+1}} \end{aligned} \quad (4.18)$$

The time in equation 4.3 is then replaced with the strain hardening factor above.

$$\bar{\epsilon}^{cr} = A\bar{q}^n t^m = A\bar{q}^n (\bar{\epsilon}^{cr} (m+1))^{\frac{m}{m+1}} (A\bar{q}^n)^{-1} (A\bar{q})^{\frac{1}{m+1}} = (\bar{\epsilon}^{cr} (m+1))^{\frac{m}{m+1}} (A\bar{q})^{\frac{1}{m+1}} \quad (4.19)$$

Which is the same equation found in the Abaqus manual, see equation 4.12. Abaqus then solves equation 4.19 by using a numerical step by step method, same way as described for time hardening.

## Referring to EC

Similar to time hardening, the creep rate can be referred to the creep function described in EC. When load is added the creep rate will change according to Figure 4.5. The behaviour of the strain hardening model, and how the total creep can be calculated using the creep function, is shown in Figure 4.6 and in the following relations.

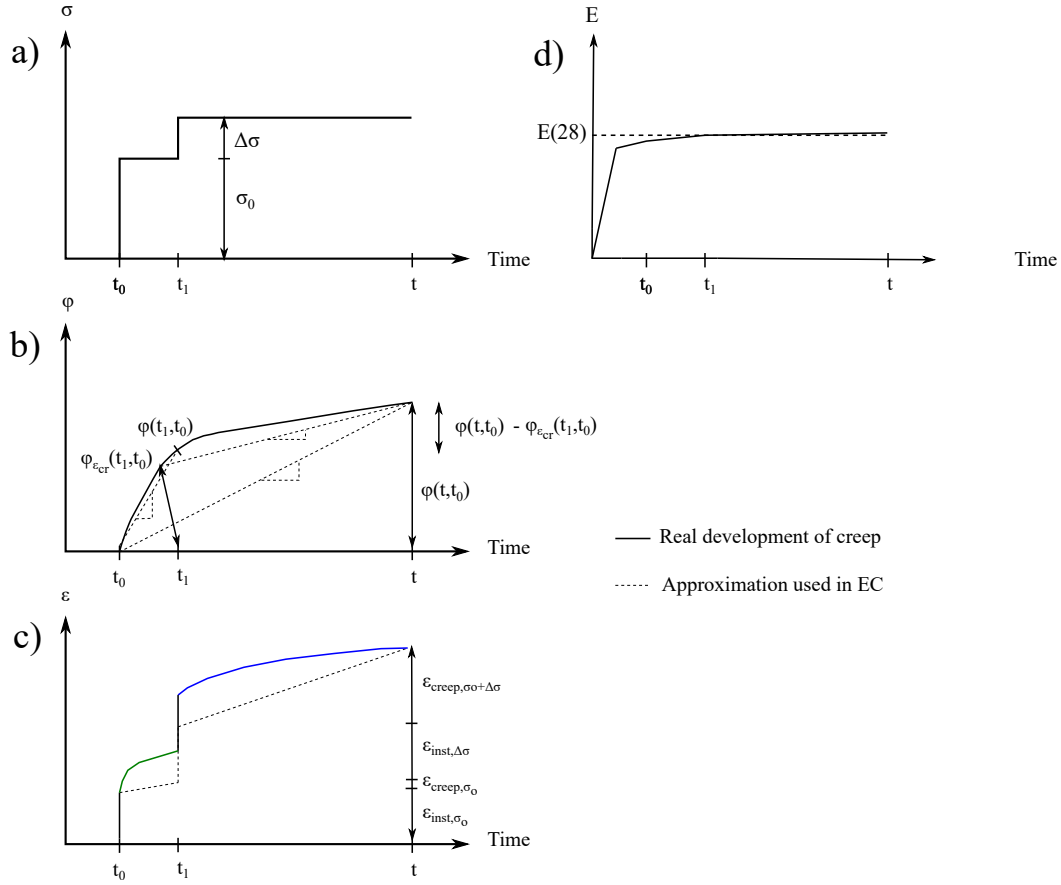


**Figure 4.6:** Showing how the stress (a), creep coefficient (b), total strain (c) and Young's Modulus (d) varies over time for strain hardening.

$$\begin{aligned}
 \epsilon_{inst,\sigma_0} &= \frac{\sigma_0}{E_c} \\
 \epsilon_{creep,\sigma_0} &= \frac{\sigma_0}{E_c} \varphi(t_1, t_0) \\
 \epsilon_{inst,\Delta\sigma} &= \frac{\Delta\sigma}{E_c} \\
 \epsilon_{creep,\sigma_0+\Delta\sigma} &= \left( \frac{\sigma_0}{E_c} + \frac{\Delta\sigma}{E_c} \right) (\varphi(t, t_0) - \varphi_{cr}(t_1, t_0))
 \end{aligned} \tag{4.20}$$

The creep coefficient,  $\varphi_{cr}(t_1, t_0)$  marks from where along the curve of the creep function, illustrated in Figure 4.6, creep will continue to develop after the load has increased. It can be decided by setting the creep strains equal for the previous and current load as:

$$\frac{\sigma_0}{E_c} \varphi(t_1, t_0) = \frac{\sigma_0 + \Delta\sigma}{E_c} \varphi_{cr}(t_1, t_0) \Rightarrow \varphi_{cr}(t_1, t_0) = \frac{\sigma_0}{\sigma_0 + \Delta\sigma} \varphi(t_1, t_0) \tag{4.21}$$

The sum of the strain eq 4.22, can be related to the General and incremental step-by-step method described in EC, similar to time hardening. It should be noted, however, that if further loads are applied the creep coefficient  $\varphi_{\epsilon_{cr}}$  becomes complicated to calculate by hand, it can instead be determined numerically.

$$\epsilon(t) = \frac{\sigma_0}{E_c} [1 + \varphi(t, t_0) + \varphi_{\epsilon_{cr}}] + \sum_{i=1}^n \frac{\Delta\sigma_i}{E_c} [1 + \varphi(t, t_0) - \varphi_{\epsilon_{cr}}(t_i, t_0)] \quad (4.22)$$

### 4.2.3 Calibrating Time and Strain Hardening Parameters

When using time/strain hardening, only one creep function is used to calculate the creep strain for all loads that are applied over time. The creep function is calculated based on the age of the concrete when the first load is applied,  $t_0$ . Concrete as a structural member can be seen as isotropic (Reiner, 1949), which entails that the equation used in Abaqus to calculate the creep strain, can be changed to equation 4.9, according to section 4.2.1. The parameters used in the equation can then be found by comparing it to the general creep strain equation described in Eurocode 2 (2005a):

$$\epsilon_{cr}(t) = A\sigma^n \frac{t^{m+1}}{m+1} = \frac{\sigma \cdot \varphi(t, t_0)}{E_c} \quad (4.23)$$

The parameters can be found by using the natural logarithm and dividing the equation into sets:

$$\ln(A\sigma^n \frac{t^{m+1}}{m+1}) = \ln(\frac{\sigma \cdot \varphi(t, t_0)}{E_c}) \quad (4.24)$$

$$\ln(A) + n \cdot \ln(\sigma) - \ln(m+1) + (m+1) \cdot \ln(t) = \ln(\sigma) - \ln(E_c) + \ln(\varphi(t, t_0)) \quad (4.25)$$

The elastic modulus increases in magnitude rapidly and normally reaches its design value,  $E_{cm}$ , after 28 days (as previously discussed in section 3.2.4). Due to creep developing slowly over a long period, the elastic modulus can be simplified to be time-independent in the equations above with the value of  $E_{cm}$ . The only variable in the two equations above is the time, the parameter  $m$  can therefore be found by comparing the inclination, principle of calibrating  $m$  is shown in Figure 4.7.

$$(m+1) \cdot \ln(t) = \ln(\varphi(t, t_0)) \quad (4.26)$$

The other parameters,  $A$  and  $n$ , can be found by putting the constants equal in equation 4.25:

$$\ln(A) - \ln(m+1) + n \cdot \ln(\sigma) = \ln(\sigma) - \ln(E_c) \quad (4.27)$$

The equation above should hold for all magnitudes of the stress,  $\sigma$ , indicating that the value of  $n$  should be one or close to one. The parameter  $A$  is then determined as:

$$\ln(A) = -\ln(E_c) + \ln(m+1) \quad (4.28)$$

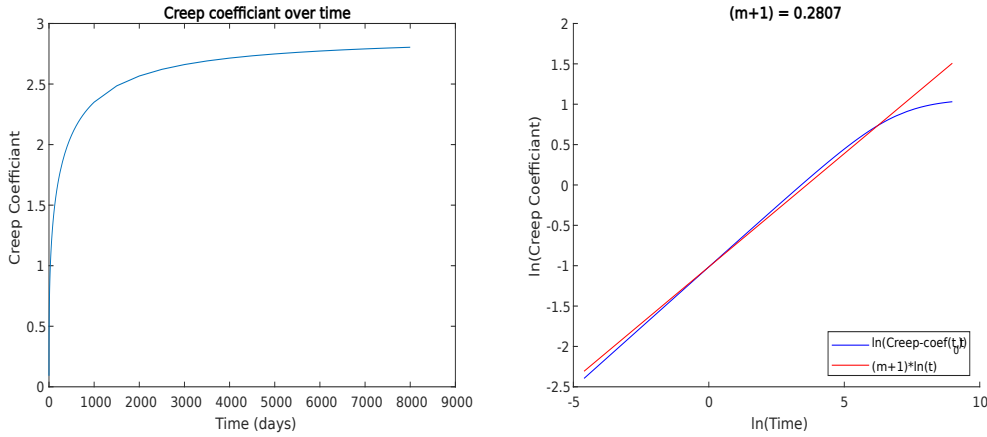


**Figure 4.7:** Left: development of the creep coefficient over time. Right: comparison of the creep coefficient and the time dependent part of the equation in Abaqus, using a logarithmic scale.

### 4.2.4 Viscoelastic Model

A viscoelastic material is characterised by a combination of two theories. Viscosity, which describes how a fluid resists flow (compare for example honey and water) and Elasticity which describes how a material deforms under load (compare for example steel and timber). This means that a viscoelastic material is subject to both instant (Elasticity) and time-dependent (Viscosity) strain (Ohlsson, 2018).

As described in for example Grasley and Lange (2007), the ageing, viscoelastic behaviour of concrete is due to the properties of the cement paste. Whereas the aggregates are known to behave elastically and in a non-aging manner. The studies regarding this subject have primarily been performed with the goal to understand the long-term deformations in concrete. Which is also why it has been considered as an appropriate model to determine the creep behaviour.

### Viscoelastic modelling in Abaqus

Abaqus allows for a viscoelastic material model, see section 22.7.1 "Time Domain Viscoelasticity" in Simulia (2014). The material is described by several Prony series expansions that describes the stress relaxation during a one-dimensional stress test (The strain is kept constant). This is basically a generalization of the Maxwell model which consists of a viscous damper and an elastic spring connected in series (see Figure 4.8).

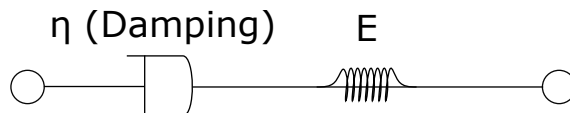


**Figure 4.8:** Principle of the Maxwell model to determine viscoelastic properties.

The Prony series expansion of the normalized shear modulus,  $g_R$ , is shown below. A similar expression exists for the volumetric response (connected to the normalized bulk modulus,  $k_R$ ).

$$g_R(t) = 1 - \sum_{i=1}^N \bar{g}_i^P (1 - e^{-t/\tau_i^G}) \quad (4.29)$$

In Abaqus it is possible to define this behaviour in several ways:

- Direct specification - Define required parameters for each term in the Prony series expansion. Since these are quite difficult to determine this method is not considered.
- Creep test data - The creep test data is converted to relaxation data and then to the Prony series parameters using a nonlinear least-square fit.
- Relaxation test data - A nonlinear least-square fit is used to convert the relaxation test data into the Prony series parameters.

### Creep test data

The normalized shear and bulk compliance ( $j_S$  &  $j_K$ ) are defined as:

$$j_S(t) = G_0 J_S(t) \quad \text{and} \quad j_K(t) = K_0 J_K(t) \quad (4.30)$$

where  $J_S(t) = \gamma(t)/\tau_0$  and  $J_K(t) = \epsilon^{vol}(t)/p_0$  are the shear and bulk compliance.  $G_0$  and  $K_0$  are the shear/bulk modulus at time  $t = 0$ , at  $t = 0$  the factors  $j_S = j_K = 1$ . Furthermore, we recall the following definitions for an isotropic material (Eurocode 2, 2005a).

$$G_0 = \frac{E_0}{2(1 + \nu_0)} \quad \text{and} \quad K_0 = \frac{E_0}{3(1 - \nu_0)} \quad (4.31)$$

### Relaxation test data

For small strains, the dimensionless shear relaxation modulus,  $g_R$ , is defined as:

$$g_R(t) = G_R(t)/G_0 \quad (4.32)$$

where  $G_R$  is the time-dependent shear relaxation modulus,  $G_R(0) = G_0$ .

The creep coefficient,  $\varphi(t, t_0)$ , can be implemented according to Eurocode 2 (2005a) section 7.4.3 (Using the effective modulus of elasticity,  $E_{c,eff}$ ). It is also recognised that Poisson's ratio,  $\nu$ , does not change considerably after the concrete has cured (Allos and Martin, 1981). The shear modulus at time  $t$ ,  $G_R$ , can then be evaluated as:

$$G_R = \frac{E_{c,eff}}{2(1 + \nu)} = \frac{E_0}{1 + \varphi(t, t_0)} \frac{1}{2(1 + \nu_0)} \quad (4.33)$$

The dimensionless shear relaxation modulus,  $g_R$ , can finally be derived according to the equation below,  $k_R$  is calculated using the same principle.

$$g_R = \frac{G_R}{G_0} = \frac{\frac{E_0}{1 + \varphi(t, t_0)} \frac{1}{2(1 + \nu_0)}}{\frac{E_0}{2(1 + \nu_0)}} = \frac{1}{1 + \varphi(t, t_0)} = \frac{K_R}{K_0} = k_R \quad (4.34)$$

## 4.2.5 Comparison of Creep Models

### Comparing time and strain hardening

Using the time or strain hardening model gives different results if the stress changes over time. The difference stems from how the models calculate the change in creep rate due to change in load, as illustrated conceptually in Figure 4.9 and 4.10. It is clearly shown that the strain hardening model results in greater creep rate, resulting in larger creep strains if the stress is increased.

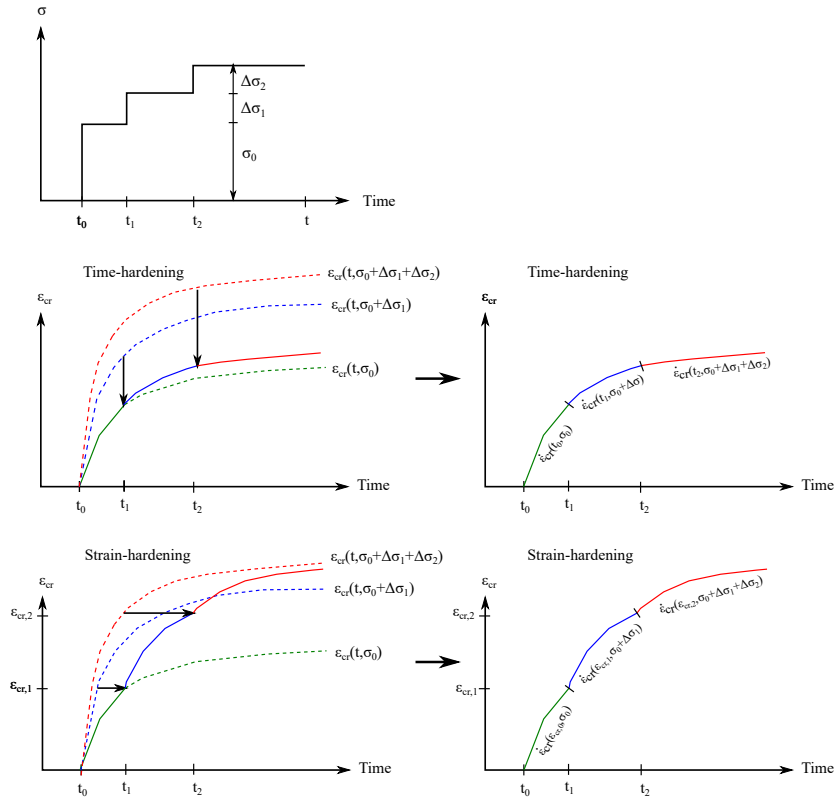


**Figure 4.9:** Comparison of total strain caused by load being applied at  $t_0$  and  $t_1$ , using both a time and strain hardening model.

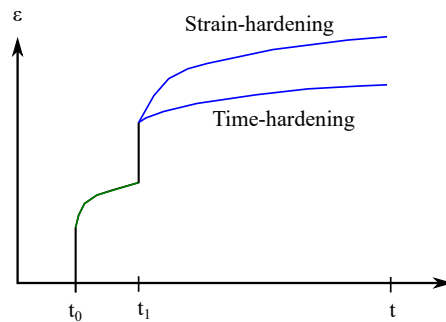


**Figure 4.10:** Difference in total strain, based on using a time or strain hardening model.

## Numerical comparison of all three models

The result achieved by using a time or strain hardening model are very sensitive to change in their parameters. The size of the time steps and tolerance values needed to perform the analysis also vary greatly depending on the choice of parameters. This indicates that the parameters must be decided with good precision in order to achieve a good result, which is both difficult and time consuming.

For the viscoelastic model, the only parameter needed is simply the creep function according to EC, which makes the viscoelastic model much easier to use. Furthermore, this model is considerably less sensitive to the size of time steps and tolerance values.

### 4.3 Verification of Creep Models

The creep models were verified by using a simple example of a concrete cube subjected to a uniform tension, see Figure 4.11. The cube had the same properties as the bridge girder in the case study, see section 6.2. A tensile stress of 1 MPa was applied after 7 days and was then increased by 1 MPa every tenth day, to simulate a segmentally loaded structure.

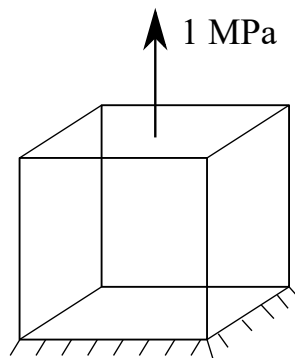


**Figure 4.11:** Simplified load case of concrete cube subjected to tension, used to verify the creep models.

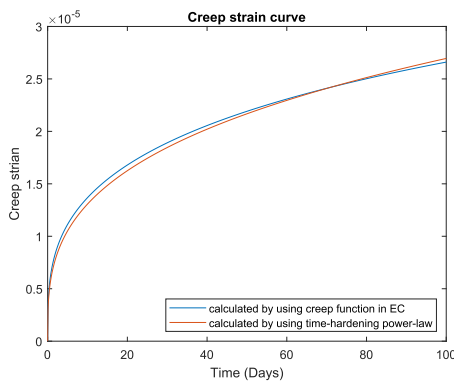
The discussed creep models were implemented in Abaqus and compared with hand calculations performed in MATLAB. The hand calculations was based on the General and incremental step-by-step method in section 4.1. This equation was considered suitable due to its simplicity as well as having the ability to adapt to the different creep theories. In the designers guide to Eurocode 2 (2005b), see Hendy and Smith (2007), this method is also explained to be the best choice for balanced cantilever constructions (as for the case study in this report). The calculations were adapted to fit the three different creep theories studied. This means that the viscoelastic model was compared to the fundamental equation described in section 4.1. Time and strain hardening were instead compared to section 4.2.1 and 4.2.2.

### 4.3.1 Time and Strain Hardening Model

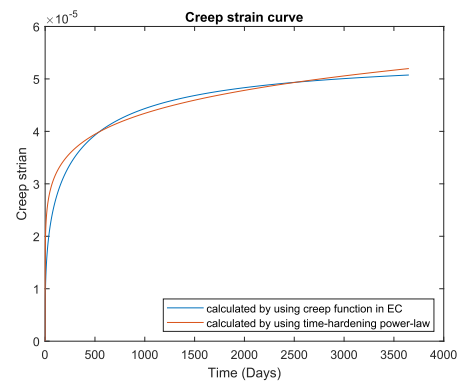
The power law parameters were chosen to fit the development of creep strain according to EC. The chosen parameters are shown in Table 4.1 and Figure 4.12. Due to difficulties in describing the development with time, both short- and long-term parameters were calibrated.

**Table 4.1:** Parameters chosen in Abaqus for time/strain hardening model.

	A	n	m
Long time (10 years)	1.527e-12	1.03	-0.8614
Short time (100 days)	3.462e-12	0.96	-0.6857



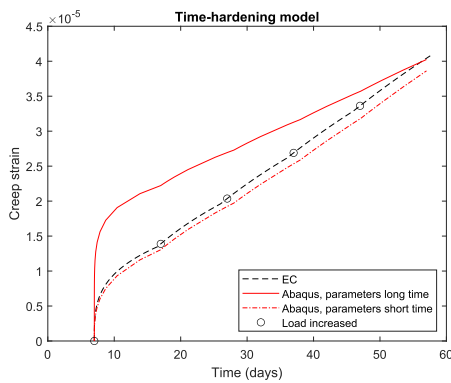
(a) Calibration of short-term parameters.



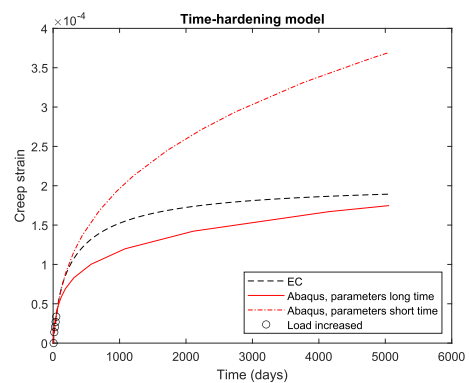
(b) Calibration of long-term parameters.

**Figure 4.12:** Parameters calibrated to the creep function from EC by looking at a short and long period of time.

Using the calibrated parameters, an investigation was made how the time and strain hardening models behaved when loads were incrementally applied over time. The results are shown in Figure 4.13 and 4.14. From the figures it can be noted that the models are in reasonably good compliance with the adapted theory from EC, see eq 4.11 and 4.22.



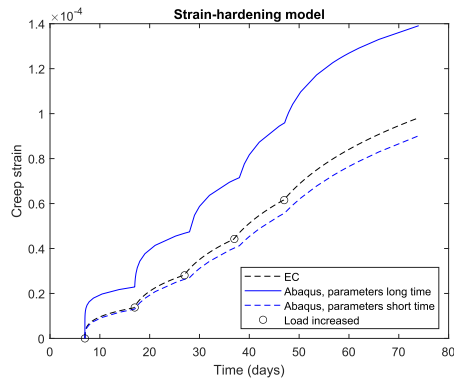
(a)



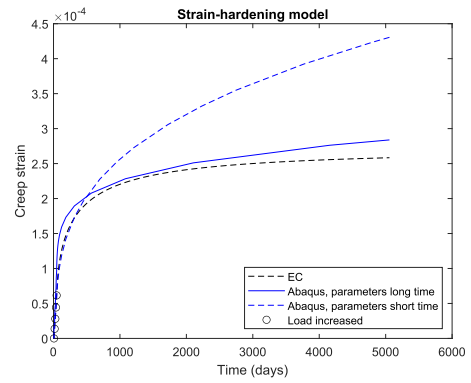
(b)

**Figure 4.13:** Comparing time hardening model in Abaqus to the adapted theory from EC (see eq 4.11).





(a)



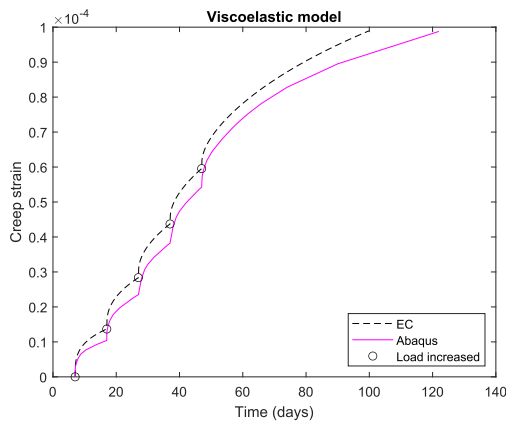
(b)

**Figure 4.14:** Comparing strain hardening model in Abaqus to the adapted theory from EC (see eq 4.22).

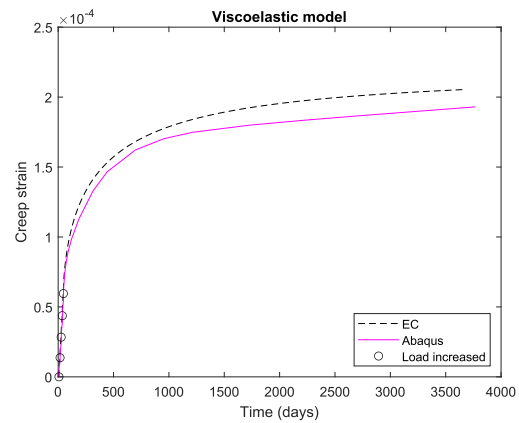
### 4.3.2 Viscoelastic Model

The viscoelastic model was implemented in the same way as for the case study, section 6.2. It is compared with the theory from EC and equation 4.1 (Not accounting for shrinkage), the result is shown in Figure 4.15. A couple of advantages with this model can be noted:

- The creep strains follow the development from EC very well.
- The method is simple, as there is no need to calibrate any parameters.
- The model, in Abaqus, runs faster compared to time and strain hardening.



(a)



(b)

**Figure 4.15:** Comparing viscoelastic model in Abaqus to the theory from EC (see eq 4.1).

### 4.3.3 Comparing Models when Unloading

The fact that the creep strain reverts when the structure is unloaded was only captured in one of the creep models, the viscoelastic model. This is illustrated in Figure 4.16, where the structure was unloaded after 5000 days.

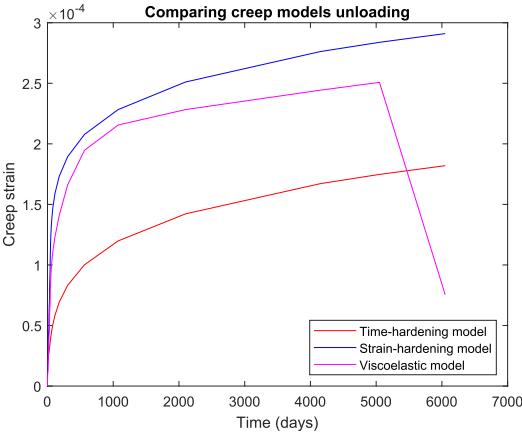


**Figure 4.16:** Comparing creep models, first ramping up the load and then unloading after 5000 days.

The creep strain rate in the two other models was not affected by the fact that the load was removed. In the case study, the permanent load is incrementally increased during construction and then held constant during the service life of the bridge. The fact that these two models do not capture the creep behaviour while unloading, might therefore not have a large impact.

### 4.3.4 Development of Young’s Modulus

By using the mean value of the Young’s Modulus,  $E_{cm}$ , there is a slight error in the elastic strains. The error is, however, considered to be neglectable. This can be seen in Figure 4.17, where the use of the actual Young’s Modulus is compared with the use of the mean value.

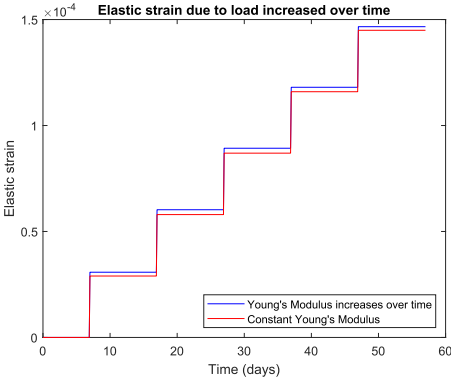


**Figure 4.17:** Resulting elastic strain by gradually increasing the load, using a time-dependent and constant Young’s Modulus.

### 4.3.5 Conclusion of Model best fit for Predicting Creep According to Eurocode

The result from the three different models were compared with the curve achieved by using the fundamental creep behaviour according to EC (as mentioned previously). This means that a unique creep function was calculated for each load, depending on the age of the concrete when the load was applied ( $t_0$ ). The results are shown in Figure 4.18 and 4.19.

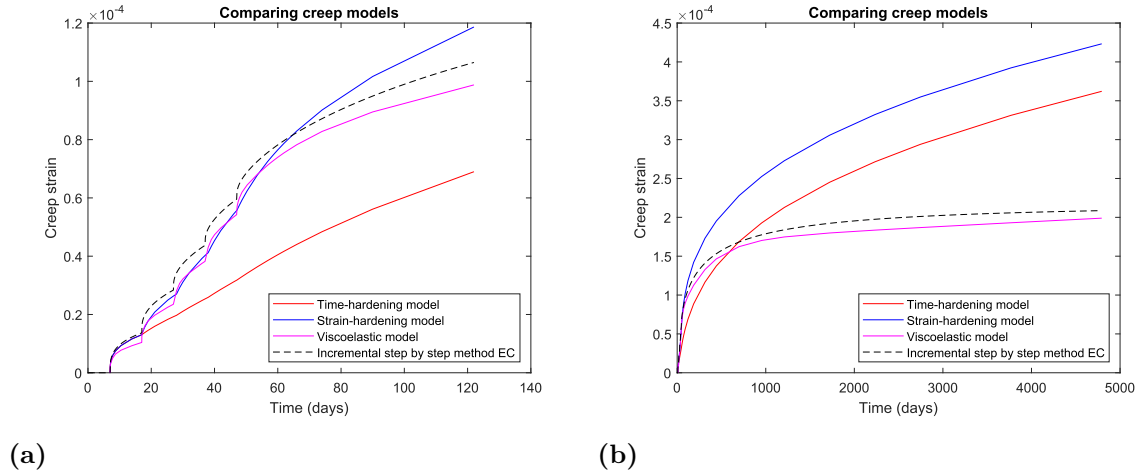


**Figure 4.18:** Comparing the three models with the theory from EC (see eq 4.1). Short-term calibrated parameters are used for time and strain hardening.

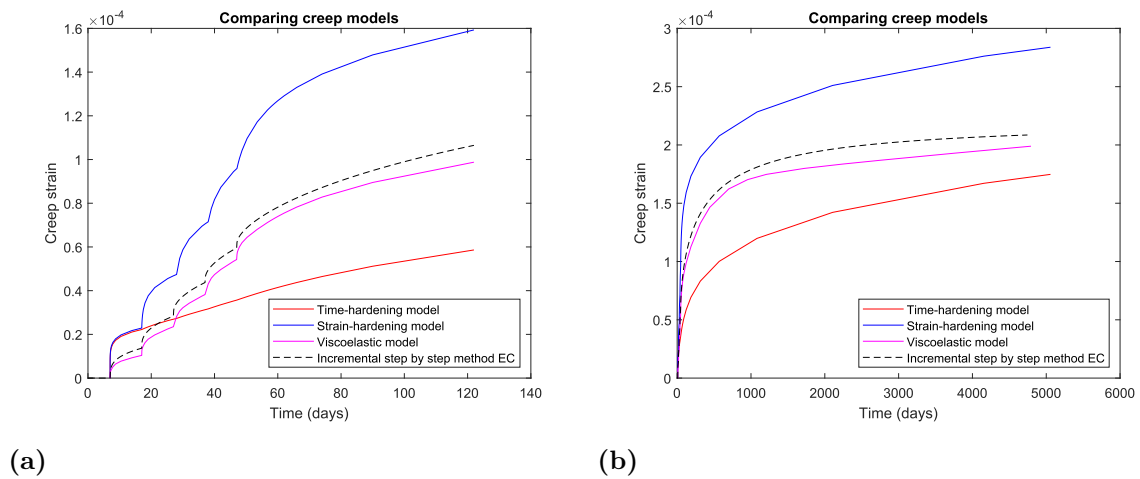


**Figure 4.19:** Comparing the three models with the theory from EC (see eq 4.1). Long-term calibrated parameters are used for time and strain hardening.

It is quite evident from Figure 4.18 and 4.19, that the creep deformation curve obtained by using the viscoelastic model follows closest the curve from EC. Therefore, it will be used to model creep in the case study. The parameters needed in the viscoelastic model are also easy to calibrate and the model is easy to run in Abaqus, as previously discussed. The predictions were slightly lower compared to EC but it should be noted that this comparison in itself is a simplification. As shown in 3.2.3 the actual creep behaviour is quite complicated to predict.



**Part II**

**Case Study**



# 5 Jiang Jin Bridge Description

A section of the Jiang Jin Bridge, built 1997 in Chongqing, China, will be studied with respect to long-term effects in order to verify the viscoelastic creep model. The bridge was selected as a suitable case study due to its simplicity, well documented properties, and reliable measurements over a long time. The structure is a segmentally cast, concrete box girder, which is a commonly used option for bridges with similar ranges of spans. A famous example is the previous Koror-Babeldaob Bridge in Palau, mentioned in the introduction of this report. The Jiang Jin Bridge is constructed using the balanced cantilever method, which is further described in 2.2.2. Dimensions and material properties are retrieved from Huang et al. (2018). Certain simplifications and assumptions are made, these are explained throughout the bridge description and modelling sections.

## 5.1 Dimensions and Positioning of Tendons

The longitudinal section of the bridge with measurements and segments is shown in Figure 5.1. Cross sections over the support and in the mid-span are shown in Figure 5.2 (only showing half of the cross section). The far-left segment rests on a land support and the far-right is connected to a mirrored section. The following assumptions were made regarding the dimensions of the Jiang Jin Bridge:

- The height of the cross section was assumed to follow a constant radius from the support to the mid-span section.
- The cross sections were reproduced from Huang et al. (2018). To simplify, the dimensions of the top flange were assumed to be constant, while the thicknesses of the bottom flange and the web were assumed to vary linearly.

The positioning of post-tensioning tendons is shown in Figure 5.3 (longitudinal) and 5.4 (cross section). Each segment in the balanced cantilever phase is prestressed with 4 top tendons (2 in this model since symmetry is being used). The closure segments are connected to the structure by tensioning the bottom tendons. Each top duct consists of 25 tendons with a nominal diameter of 15.2 mm ( $3504 \text{ mm}^2$ ) and bottom ducts consists of 19, 15.2 mm tendons ( $2663 \text{ mm}^2$ ). The following assumptions were made regarding the prestressing tendons:

- Based on the provided information, the tendons were placed to fit in the cross section, the exact placement of these were not known.
- The tendons, when looked from above, were assumed to be straight. In reality the tendons would be positioned differently to make space for the anchorage.

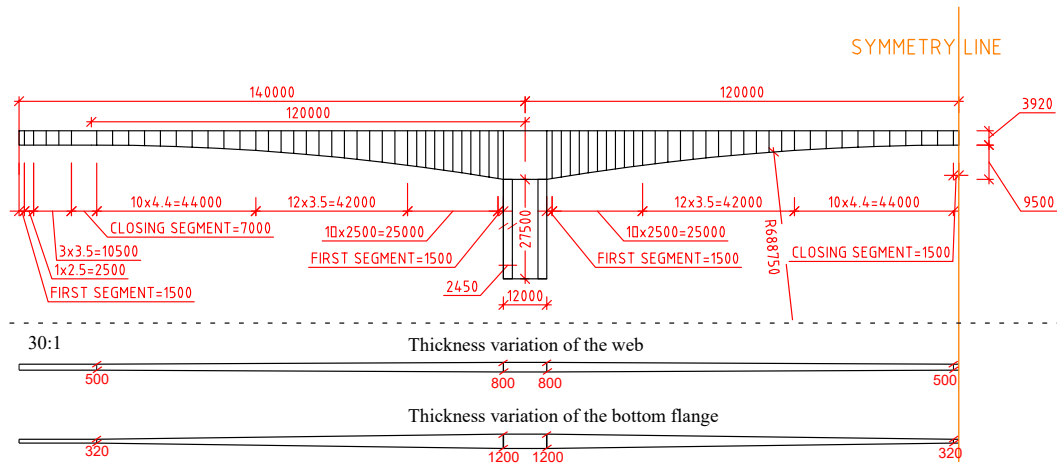


**Figure 5.1:** Longitudinal section of Jiang Jin Bridge that is studied. All dimensions are in mm.

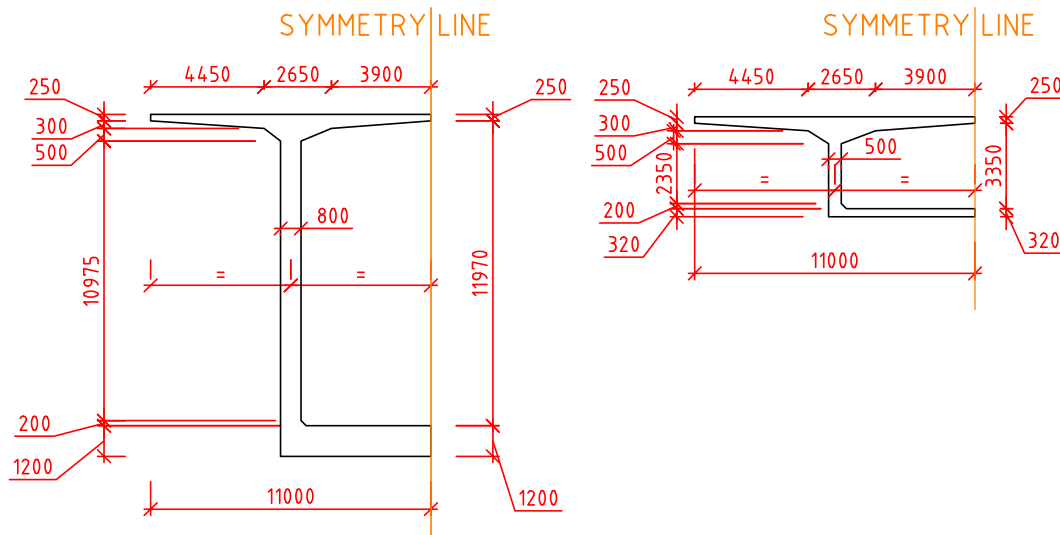


**Figure 5.2:** Cross sections of Jiang Jin Bridge, over support (Left) and at midspan (Right), a linear variation in thickness is assumed between these. All dimensions are in mm.

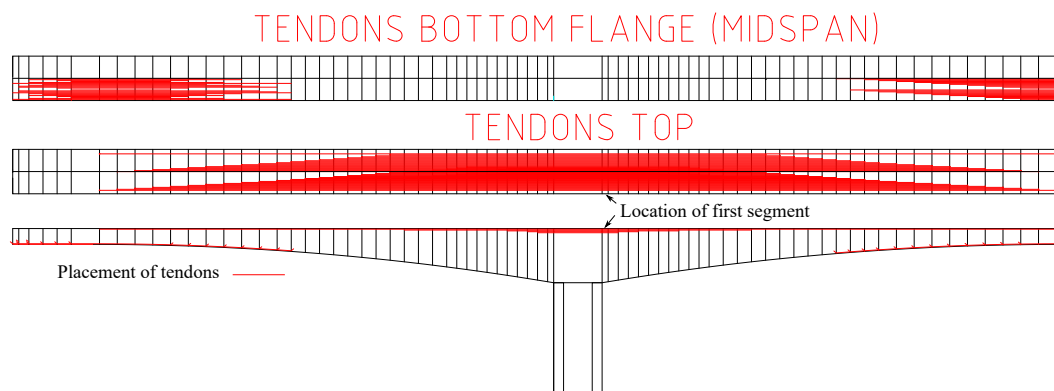


**Figure 5.3:** Positioning of tendons along the longitudinal bridge section. The two top figures show the bridge deck and how the tendons are placed horizontally.



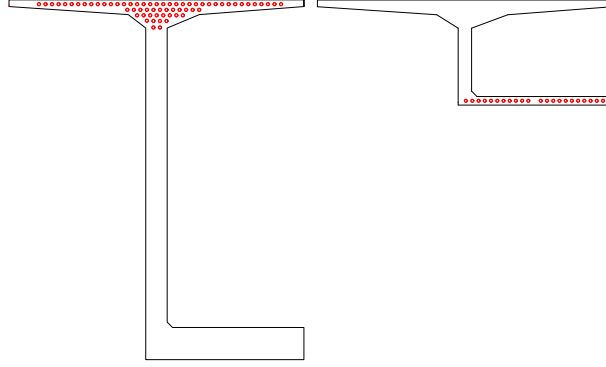


**Figure 5.4:** Positioning of top tendons over support section (left) and bottom tendons in the span (right).

## 5.2 Properties

Material properties and permanent loads of the bridge are shown in Table 5.1 and 5.2. For the material properties an assumption was made that the curing age was the same for all segments. Regarding the loads, the weight of the superstructure (pavement/parapet) had to be estimated. The weight of the travelling formwork was also neglected based on only permanent loads being relevant for the long-term behaviour of the bridge.

**Table 5.1:** Material properties of the Jiang Jin Bridge (Huang et al., 2018).

Material	Property	Value
Concrete	Bridge Girder $f_{cm,28d}$	48 MPa
	Pylons $f_{cm,28d}$	40 MPa
	Bridge Girder $E_{cm}$	34.5 Gpa
	Pylons $E_{cm}$	32.5 Gpa
	Curing age $t_0$	7 Days
	RH (Relative Humidity)	70 %
	$\alpha$ (Concrete)	1e-5 (Standard)
Post-tensioning Tendons	Tensile strength $f_{puk}$	1860 MPa
	Initial tendon stress $\sigma_{pi}$	1395 MPa
	$E_p$	195 Gpa
	$\alpha$ (Steel)	9e-6 (Standard)

**Table 5.2:** Loads of the Jiang Jin Bridge

Type	Value
Concrete density	2500 kg/m <sup>3</sup>
Superstructure weight	2.5 kPa (Estimated)
Post-tensioning tendons (weight)	Neglected
Formwork and scaffolding	Neglected

## 5.3 Construction Sequence

The concrete segments were cast-in-situ in a balanced cantilever construction. Regarding the long-term effects, changes in the timeline of the cantilever construction, prestressing sequence, and closure segments can have a large impact. The matter in which the pylons and midsection are constructed are less important in this regard. The following timeline is given by Huang et al. (2018):

1. The balanced cantilever construction was completed,  $t = 300$  days. Progress is shown in Figure 5.5.
2. The side-span (left) closure segment was cast and bottom tendons were prestressed from one side,  $t = 310$  days. Progress is shown in Figure 5.6.
3. The mid-span (right) closure segment was cast and the bottom tendons were prestressed from both sides,  $t = 320$  days. Progress is shown in Figure 5.7.
4. The remaining superstructure such as pavement was added,  $t = 350$  days.

In addition to the timeline above, some assumptions had to be made in order to model the construction sequence:

- Each segment took 9 days to cast and prestress.
- The segments left of the side-span were assumed to be cast on temporary supports, before the closure segment since these were over land.
- Measurements of the relative elevations were initiated at mid- and side-span after the weight of the remaining superstructure was added, at  $t = 360$  days.

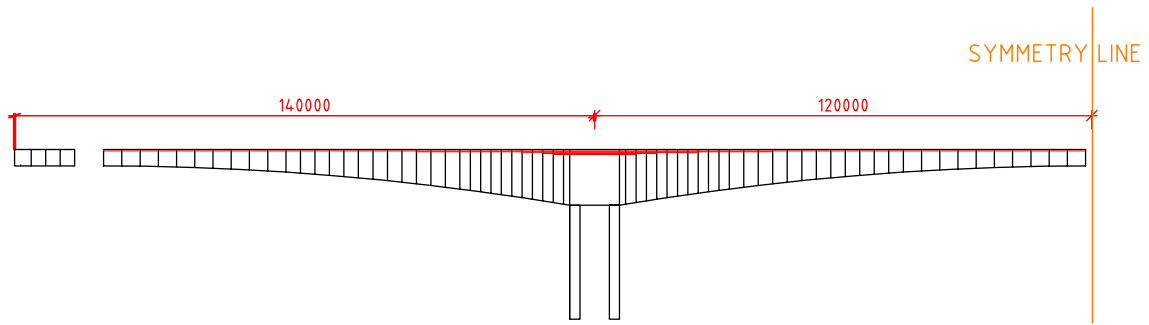


**Figure 5.5:** Construction progress after 300 days. Completed cantilever construction and left support segments are cast on temporary supports.

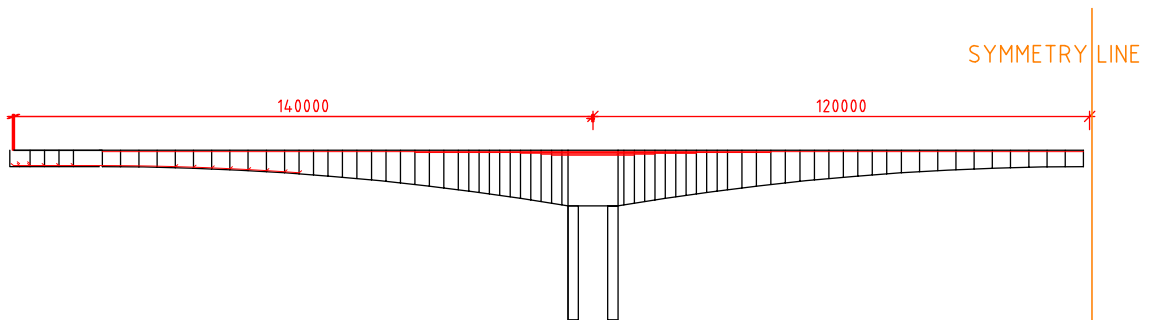


**Figure 5.6:** Construction progress after 310 days. Closure segment for the side-span is cast and bottom left tendons are prestressed, temporary supports are removed.

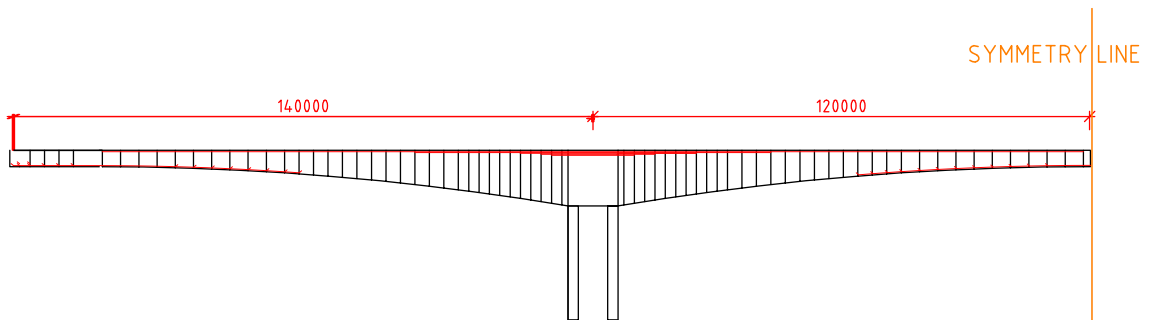


**Figure 5.7:** Construction progress after 320 days. Closure segment for the mid-span is cast and bottom right tendons are prestressed.



## 6 Finite Element Model

The Jiang Jin Bridge was modelled using shell and beam elements (see Figure 6.1 and 6.2). Two symmetry conditions exist which allowed for only half of the bridge to be modelled, which significantly reduced the calculation and modelling times. The blue line in Figure 6.1 represents the symmetry condition at the mid-section of the bridge deck (still allowing for longitudinal and vertical movement). This was possible since the bridge girder is symmetric in the transverse direction and only permanent loads were considered. The symmetry condition to the right was modelled as a rigid connection, but with the ability to move in the vertical direction. The left support was modelled with a roller bearing and the foundations of the pylons with a rigid connection.

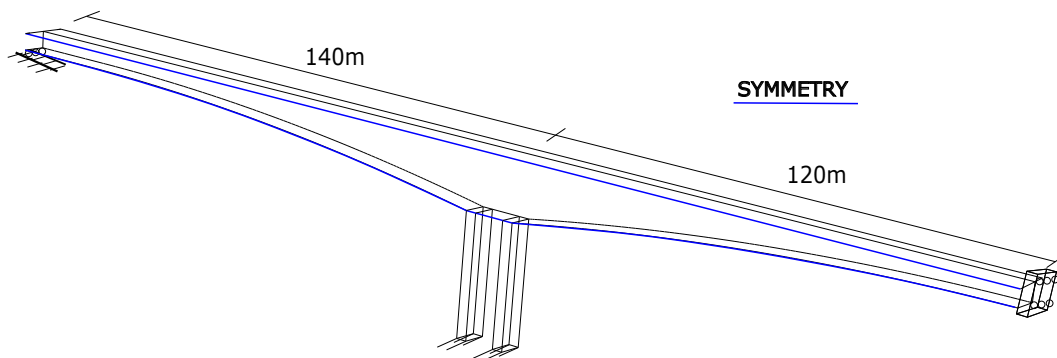


**Figure 6.1:** Shell model showing the boundary conditions, including the symmetry.

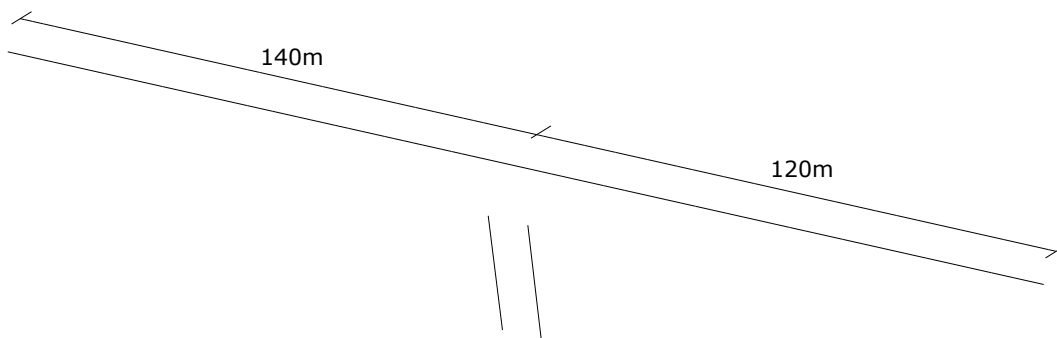


**Figure 6.2:** Beam model, same boundary conditions as for the shell model.

Shell elements capture important 3D effects like shear lag, while also keeping the calculation time to a reasonable level. This was the first choice of approach to model the long-term effects. The dimensions were modelled according to chapter 5, with the exception that the top flange was modelled with a constant thickness. Modelling with beam elements is, however, often the preferred approach due to its simplicity. The main advantage of using beam elements is that the geometry is not modelled explicitly, i.e. the cross-sectional properties are calculated separate from the 3D model and can therefore easily be changed. The geometry had to be simplified further for the beam model, each segment being modelled as an I beam with constant dimension.

## 6.1 Modelling of Shrinkage

As described in section 3.2.2, the autogenous shrinkage depends only on the concrete quality and elapsed time since casting. The drying shrinkage, however, also depends on the notional size of the cross section, which means that sections along the bridge girder will have different shrinkage properties. Table 6.1 shows the total shrinkage strain for different notional sizes and time steps. The calculations were based on the theory described in section 3.2.2, using the parameters of the Jiang Jin Bridge. It can be noted that the final shrinkage does not vary a lot with different notional sizes. The rate, however, varies quite significantly (compare the shrinkage strains at for example  $t=50$  days).

**Table 6.1:** Total shrinkage strain calculated for different notional sizes and times steps (in days).

$h_0$ [mm]	$\epsilon_{cs}$ [‰]				
	t=10	t=50	t=250	t=1000	t= $\infty$
100	0,052	0,219	0,344	0,381	0,394
200	0,037	0,125	0,252	0,315	0,344
300	0,033	0,090	0,194	0,268	0,311
500	0,031	0,068	0,141	0,222	0,294

Shrinkage strains were modelled by applying a negative temperature corresponding to  $T = \epsilon_c/\alpha$ , where  $\alpha$  is the temperature coefficient. The temperature varied with time and was implemented by using an amplitude function (tabular). The shrinkage for segment 1 was added after the casting of segment 2 had begun, to best match the actual process. The bridge girder needed to be divided into several different segments, with different notional sizes. For this case study, the following simplifications were made to reduce modelling time:

- The notional size was assumed to be 500 mm, an average value to represent the whole bridge girder (510 mm according to Huang et al. (2018)).
- Shrinkage in the transverse direction were neglected.

## 6.2 Implementation of Creep in Abaqus

The Abaqus relaxation test data was used to model the concrete viscoelastically, the parameters needed were  $g_R$ ,  $k_R$  and the respective time step  $t$ . By using the simplified equation for these parameters, see section 4.2.4, as well as the basic creep theory in 3.2.3, these could be determined for a number of time steps. An example is shown in the calculations below and in Table 6.2, using the parameters of the Jiang Jin Bridge:

- $t_0 = 7$  (Loading after 7 days),  $t = 100$  days
- Notional size,  $h_0 = 500$  mm (Simplification),  $RH = 70$  %,  $f_{cm} = 48$  MPa
- $\alpha_1/\alpha_2/\alpha_3$  are given in Eurocode 2 (2005a)

$$\alpha_1 = \left[ \frac{35}{f_{cm}} \right]^{0.7} = 0.80 \quad , \quad \alpha_2 = \left[ \frac{35}{f_{cm}} \right]^{0.2} = 0.94 \quad (6.1)$$

$$\varphi_{RH} = \left[ 1 + \frac{1 - RH/100}{0.1 \sqrt[3]{h_0}} \alpha_1 \right] \alpha_2 = 1.22 \quad (6.2)$$

$$\beta(f_{cm}) = \frac{16.8}{\sqrt{f_{cm}}} = 2.42 \quad , \quad \beta(t_0) = \frac{1}{(0.1 + t_0^{0.20})} = 0.63 \quad (6.3)$$

$$\Rightarrow \varphi_0 = \varphi_{RH} \cdot \beta(f_{cm}) \cdot \beta(t_0) = 1.88 \quad (6.4)$$

$$\alpha_3 = \left[ \frac{35}{f_{cm}} \right]^{0.5} = 0.85 \quad \Rightarrow \beta_H = 1.5[1 + (0.012RH)^{18}]h_0 + 250\alpha_3 \leq 1500 = 995.99 \quad (6.5)$$

$$\Rightarrow \beta_c(t, t_0) = \left[ \frac{(t - t_0)}{(\beta_H + t - t_0)} \right]^{0.3} = 0.49 \quad (6.6)$$

$$\Rightarrow \varphi(t, t_0) = \beta_c(t, t_0)\varphi_0 = 0.92 \quad (6.7)$$

**Table 6.2:** Example of relaxation test data, using that  $g_R = k_R = \frac{1}{1+\varphi(t,t_0)}$ .

$g_R$ [Pa/Pa]	$k_R$ [Pa/Pa]	$t - t_0$ [days]
1	1	0 (time $t_0$ )
.	.	.
.	.	.
0.52	0.52	100
.	.	.
.	.	.

Since the creep function depends on several factors, for example notional size and concrete strength, the relaxation test data will differ along the bridge. A couple of simplifications were made, partly to reduce the modelling time but also due to modelling limitations.

- Simplification for shell model

- The thickness of the top flange was modelled to be constant along the length of the bridge, and therefore had a constant notional size.
- The thickness of the web varied linearly (0.5-0.8 m), the web was therefore divided into one part where the notional size was assumed to be constant.
- The thickness of the bottom flange varied linearly (0.32-1.2 m) and was divided into three parts where the notional size was assumed to be constant.

- Simplifications for beam model

- When beam elements were used for the modelling, each segment was simplified as an I profile. An average notional size was therefore used for each segment. With varying thicknesses in the cross section, this is quite a large simplification.

## 6.3 Modelling of Tendons

Tendons were modelled as beams, with dimensions and steel properties according to chapter 5. To achieve the prestressing effect, a negative temperature was applied to the tendons which, if they were not connected, would cause them to contract. The temperature was calculated by using  $T = \frac{\sigma_p}{E_p \alpha}$ , and decreased with time according to the relevant losses. The temperature was implemented using an amplitude function (tabular), in the same way as for shrinkage.

By connecting the tendons to the bridge deck, with a kinematically rigid connection, tension was applied to the post-tensioning tendons and compression to the concrete girder. This connection also allowed for time-dependent losses in the concrete to be transferred to the post-tensioning tendons. Figure 6.3 shows the principle of the interaction between the tendons and the concrete girder when shell elements were used for the modelling. The tendons were connected to partition lines with the same length. The same principle was implemented when beam elements were used. The procedure was, however, much less time-consuming since the tendons simply needed to be connected to segments of the same beam.

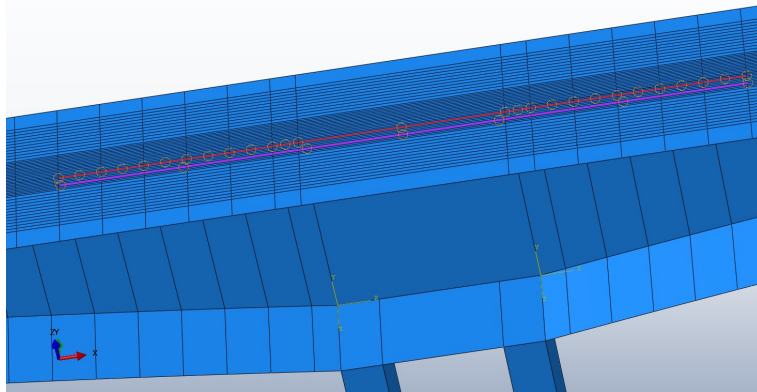


**Figure 6.3:** Interaction between bridge deck and top tendon, repeated for each tendon.

Several factors influence the effective prestressing force in the tendons. There are time-dependent losses due to steel relaxation (see section 3.2.1), and instantaneous losses due to friction and anchorage slip (see section 3.1). As the tendons are connected to the girder, strains in the concrete will also affect the prestressing force. These strains are, however, automatically considered in Abaqus due to the interaction between the tendons and the concrete girder.

### 6.3.1 Losses due to Stress Relaxation

The effective stress in the tendons,  $\sigma_p(t)$ , is calculated using the values from Table 6.3 and the method described in section 3.2.1.

**Table 6.3:** Values of the steel strands needed to calculate the relaxation factor, according to the case study and EC.

$\sigma_{pi}$ [MPa]	$f_{puk}$ [MPa]	$\chi_{1000}$
1395	1860	0.025



$$\chi_t = 0.66 \cdot \chi_{1000} \cdot e^{9.1\mu} \cdot \left(\frac{t}{1000}\right)^{0.75(1-\mu)} \cdot 10^{-3} = 0.004159 \cdot t^{0.1875} \quad (6.8)$$

where

$$\mu = \frac{\sigma_{pi}}{f_{puk}} = \frac{1395}{1860} = 0.75 \quad (6.9)$$

The effective stress is then calculated below and shown in Figure 6.4.

$$\sigma_p(t) = E_p \epsilon_{pi} (1 - 0.8 \cdot \chi_t) = \sigma_{pi} (1 - 0.003327 \cdot t^{0.1875}) \quad (6.10)$$

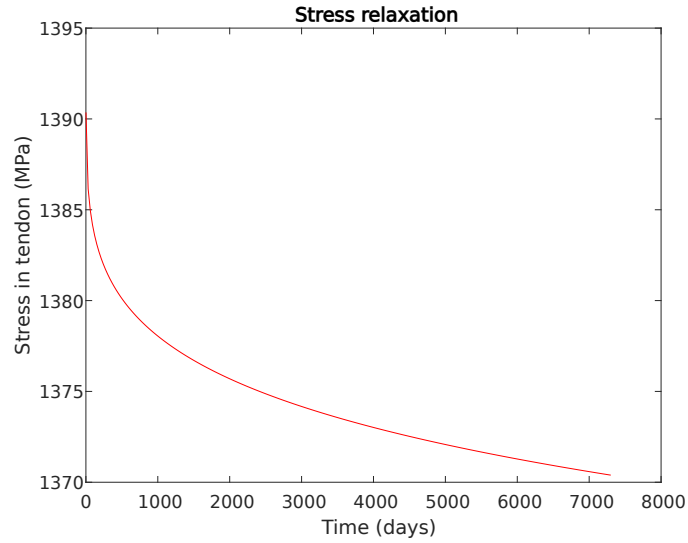


**Figure 6.4:** Stress relaxation curve of the tendons in the case studied.

### 6.3.2 Instantaneous Losses (Friction/Anchorage Slip)

The loss in the tendons due to friction,  $\Delta\sigma_\mu(x)$ , was calculated using the values from Table 6.4 and the method described in section 3.1.3.

**Table 6.4:** Value for wobble and friction coefficient for the case studied.

$k$ [rad/m]	$\mu$ [rad <sup>-1</sup> ]
0.0066	0.3

Friction losses for the top tendons are neglected since they have no curvature. The bottom tendons have a curvature as shown in Figure 6.5 and calculated as:

$$\frac{4.66}{360} \cdot 2\pi = 0.0813 \text{ Rad} \quad \Rightarrow \quad \theta = 0.0813/56 = 0.00145 \text{ Rad/m} \quad (6.11)$$

The friction losses were then calculated, assuming  $\sigma_{pmax} = \sigma_{pi}$ .

$$\Delta\sigma_\mu(x) = \sigma_{pmax} (1 - e^{-\mu(\theta+kx)}) = 1395 \cdot (1 - e^{-0.3 \cdot (0.00145 + 0.0066 \cdot 1)}) = 3.366 \text{ MPa/m} \quad (6.12)$$

### TENDONS BOTTOM FLANGE (MIDSPAN)

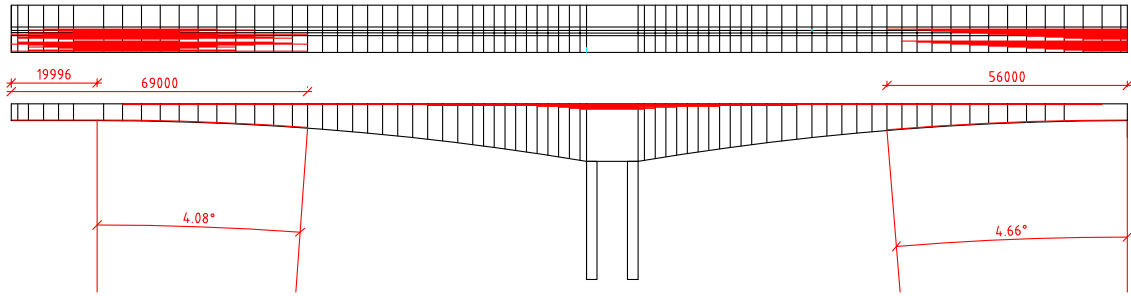
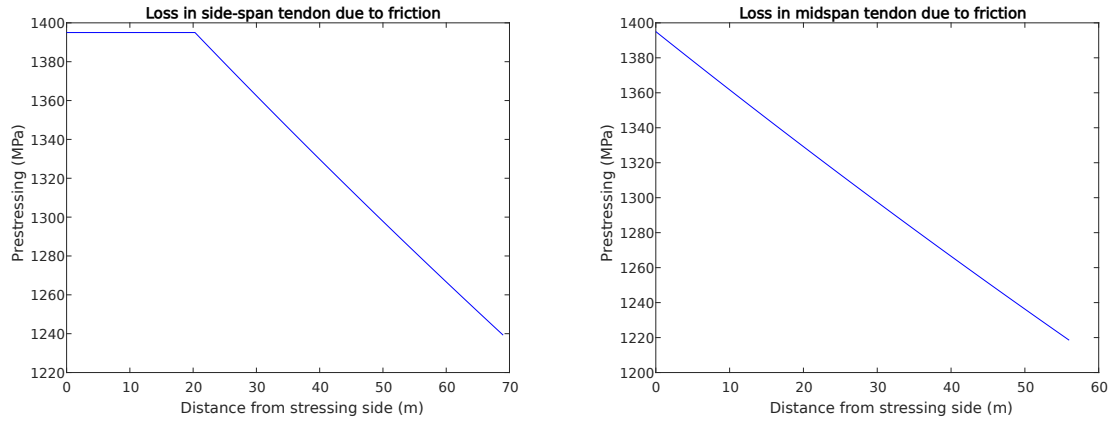


**Figure 6.5:** Figure illustrating placement and curvature of tendon located in bottom flange.

The losses in the longest bottom tendons, for mid- and side-span, are shown in Figure 6.6. Mean values of the losses in the longest/shortest tendons are presented in Table 6.5. For the modelling, a simplification was made that the stress in the tendons were reduced by 5 % to take friction and wobble into account.



(a) Side-span

(b) Mid-span

**Figure 6.6:** Losses in prestress due to friction and wobble, for the longest bottom tendons.

**Table 6.5:** Mean loss in prestressing force.

Span	Longest tendon	Shortest tendon
Side-span	5.6 %	1.2 %
Mid-span	6.4 %	2.8 %

The loss in prestressing force due to anchorage slip was calculated according to section 3.1.2 and equation 3.1. The largest loss (the shortest tendons) is calculated below, as the losses were less than 0.1 %, anchorage slip was neglected.

$$\sigma_{psl} = \sigma_{pi} \cdot \frac{d_{slip}}{L_{tendon}} = 1395 \cdot \frac{0.012}{21} = 0.8 MPa \quad (6.13)$$

## 6.4 Modelling of the Construction Sequence

To assemble the segmentally constructed bridge in Abaqus, the following steps were performed:

1. Deactivate the whole bridge with its tendons (except pylons and mid-section).
2. Activate segment.
  - Activate concrete casting.
  - Activate top tendons associated with current segment.
  - Repeat for the whole cantilever construction.
3. Activate the segments by the left support and activate the temporary supports.
4. Activate left closing segments and deactivate the temporary supports.
  - Activate concrete casting.
  - Activate bottom tendons.
  - Repeat for right closure segment.
5. Add additional permanent loads and creep for required number of days.

The correct way to model with respect to creep, would be to add the self-weight of the concrete as a load to the previous segment without activating the current casting. This is due to the concrete segment being cast not actually carrying load until the formwork is removed and the tendons tensioned. In the model used for the case study, however, the concrete segment instantly started to carry its own load.



## Part III

# Results and Discussion



# 7 Case Study Analysis

The mid- and side-span deflections were measured over time for the Jiang Jin Bridge, at the locations indicated in Figure 7.1 (Huang et al., 2018). The deflections were measured by a relative elevation study, from when the pavement and parapet were cast (day 360). The accuracy of the viscoelastic creep model was first analysed by comparing the predicted values, from the models in this case study, against the measurements. To properly verify the creep model, the deviation of the original models, compared to the provided measurements, had to be analysed. The prestressing losses in the models were finally calibrated, to better reflect the measured deflection history. Note that the time variable in this chapter is referenced from modelling time zero (construction of pylons).

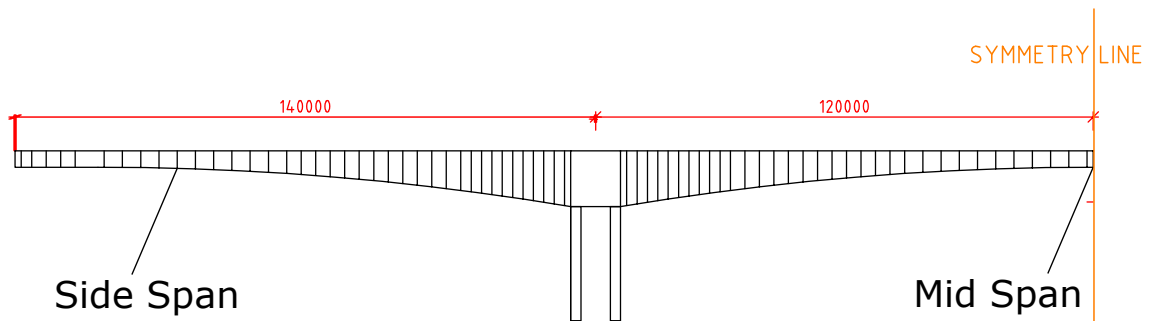
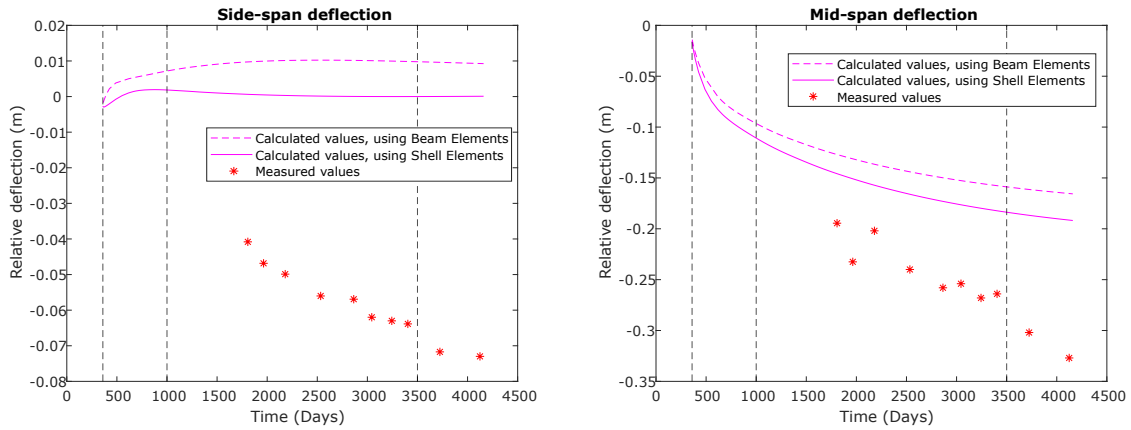


**Figure 7.1:** Locations of instruments measuring the relative deflection, at mid- and side-span.

## 7.1 Deflections

The results in Figure 7.2 show how the different models predicted mid- and side-span deflections, compared to the measured values. It can be noted that the relative long-term deformations were larger when shell elements were used. Whether this phenomenon is due to differences in the behaviour of the models, or in the implementation of the viscoelastic creep model, is difficult to interpret. It can also be noted that the measured deflection history was not reproduced. The results were, however, very similar to the numerical results originally obtained by Huang et al. (2018), prior to calibrating their model.

Figure 7.3 shows the deflections along the bridge at different time steps. This curve, however, represents the relative deflection for each segment, with respect to its casting position. This is due to Abaqus activating the segment at its undeformed location, not accounting for the deflection of previous segments. By accumulating the deflection of previous segments, the actual deflection curve was obtained in Figure 7.4.



(a) Side-span deflections

(b) Mid-span deflections

**Figure 7.2:** Comparing deflections at mid- and side-span locations. Dashed black lines show the time steps of which the deflection curves in Figure 7.3 and 7.4 are based.

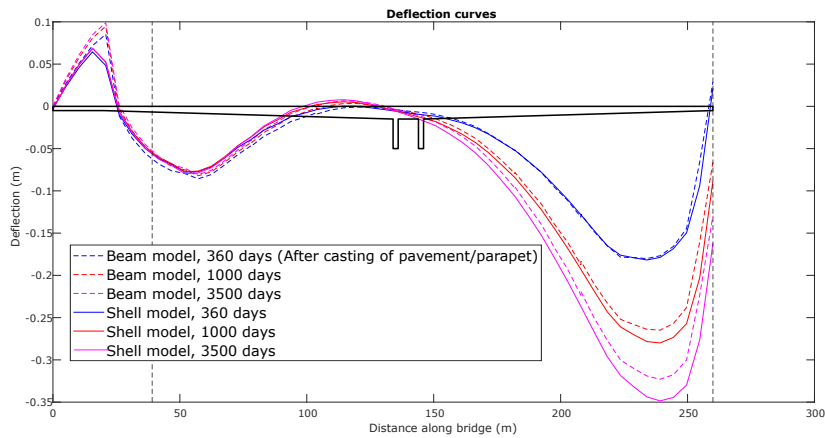


**Figure 7.3:** Deflection curves obtained from Abaqus for the shell and beam model, at different time steps. Dashed black lines show the locations where the measurements in Figure 7.2 were taken.

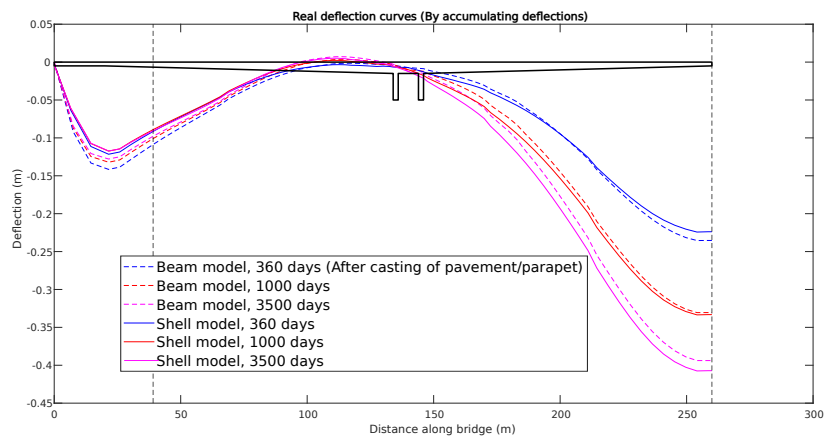


**Figure 7.4:** Actual deflection curve, obtained by accumulating deflections for previous segments.



The predicted values in Figure 7.2 to 7.4 showed an increase in deflection for the mid-span, while a decrease for the side-span (no change when shell elements were used). There are a couple of possible reasons for this phenomenon:

- The bridge will move towards the right support, due to shrinkage and concrete being compressed from prestressed tendons. As the piers are modelled as rigid to the foundation, as well as the right support being free to move in the vertical direction, the bridge will start to tilt to the right. This increases the mid-span deflection, while the deflection of the side-span is decreased. The principle of this effect is shown in Figure 7.5, where only shrinkage was considered.
- As previously mentioned, the segments are cast based on the undeformed geometry, resulting in a difference in deflection between the current and previous segment. This difference also affects the bottom tendons that connect the spans, resulting in angular deviations. By plotting the relative deflection caused by the tensioning of the bottom tendons, for the segmentally constructed bridge against a case where it was cast-in-one, the error could be analysed in Figure 7.6. The response is very similar, which implies that the angular deviations of the bottom tendons does not influence the result. A larger difference can be noted between the black solid and dashed curves, which is not surprising since the boundary condition at the mid-span is yet to be activated at this time for the segmentally constructed model.
- The effect of the tendons in the actual bridge might be lower than in the models. By comparing the difference between the two curves, illustrated in Figure 7.7, the relative deflection is obtained without regarding the effect of the tendons. The difference between these deflections and the predicted values are then because of the post-tensioning tendons. An interpretation can be made that the effect of the tendons is lower than what was modelled. Note, also, that the creep deformation is significantly larger for the mid-span.

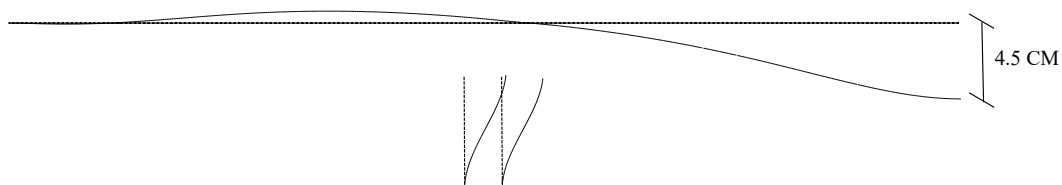


**Figure 7.5:** Deflection when only shrinkage was considered, a cast-in-one beam model was used and the analysis was performed for 3500 days.

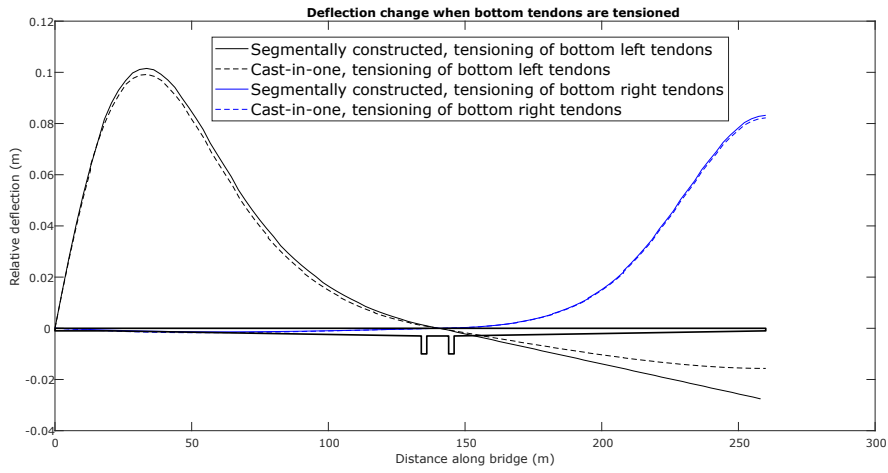


**Figure 7.6:** Effect of bottom tendons being tensioned, comparing the segmentally constructed bridge to a case where it was cast-in-one.

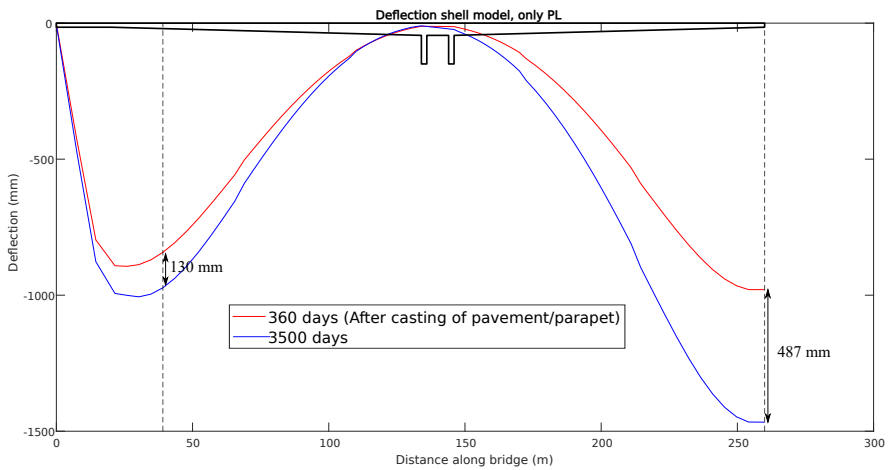


**Figure 7.7:** Real deflection when the effect of the tendons are neglected (using shell elements).

As mentioned previously, the relative long-term deformations were larger when shell elements were used. It is, therefore, of interest to analyse the difference between using shell or beam elements, whether it is due to the creep model or other factors. By plotting the deflection curves and not accounting for the creep (see Figure 7.8), it can be noted that they differ a couple of percent. It should also be noted that the total mass of the models differed by 2 %, possibly influencing the results slightly. This difference cannot, however, explain the difference in long-term deformations between the different models. Especially since the beam model predicts larger deflections than the shell model, for this case when creep was not implemented. The conclusion can be drawn that the creep model predicts larger deformations when shell elements are used. Note, however, that the implementation of the creep model was different due to differences when modelling the geometry.

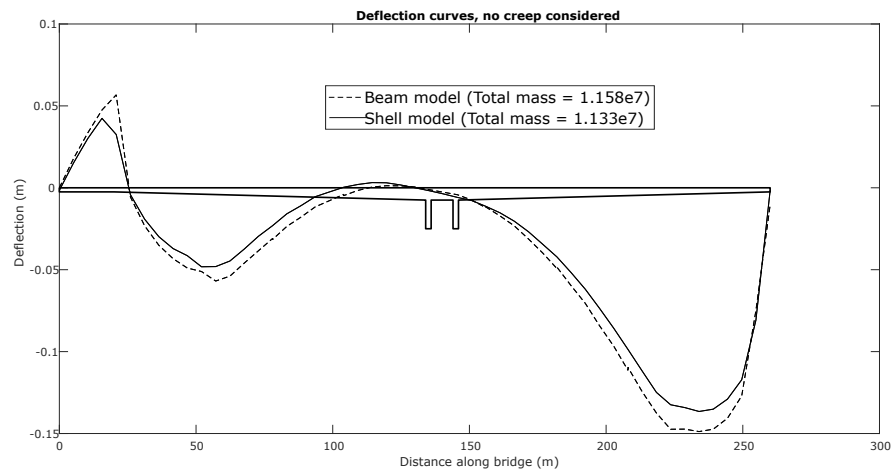


**Figure 7.8:** Deflection curve along the longitudinal section of the bridge, no creep considered.

# 7.2 Analysis of Bending Moments

To further verify that the modelling of the Jiang Jin Bridge was correctly performed, the bending moment for the beam model was analysed. The tendons were first neglected so that the behaviour described in the literature study could be seen. The tendons were then included to show the effect of prestressing.

## 7.2.1 Bending Moment due to Permanent Loads

As shown by Hendy and Smith (2007), the creep deformation for segmentally built structures redistributes the bending moment towards if it was to be built in one go. This is also the basis of the simplified method to calculate creep redistribution, see section 4.1 (Simplified ageing coefficient method). This phenomenon can be seen in Figure 7.9, where the creep redistribution is shown as the dashed black line. Furthermore, the behaviour described by Kwak and Son (2002), in section 2.2.2, can be seen in Figure 7.10. It is clearly shown that the moment over the support decreases over time while the moment in the spans increases.

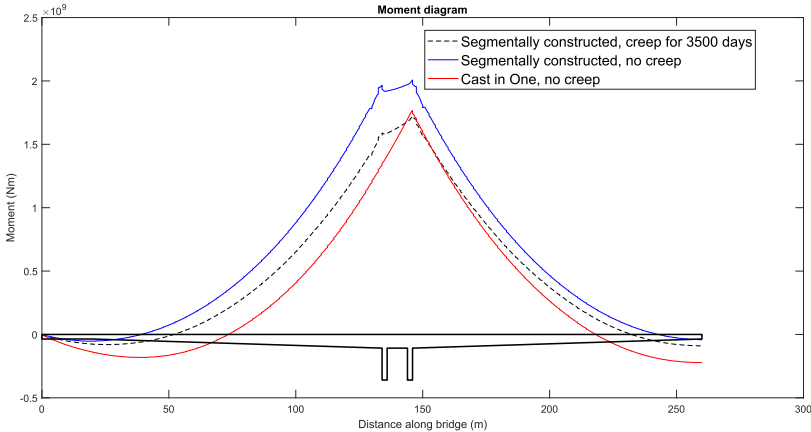


**Figure 7.9:** Bending moment when the tendons are neglected, showing the creep redistribution between the segmentally constructed bridge and the case where it was cast-in-one.

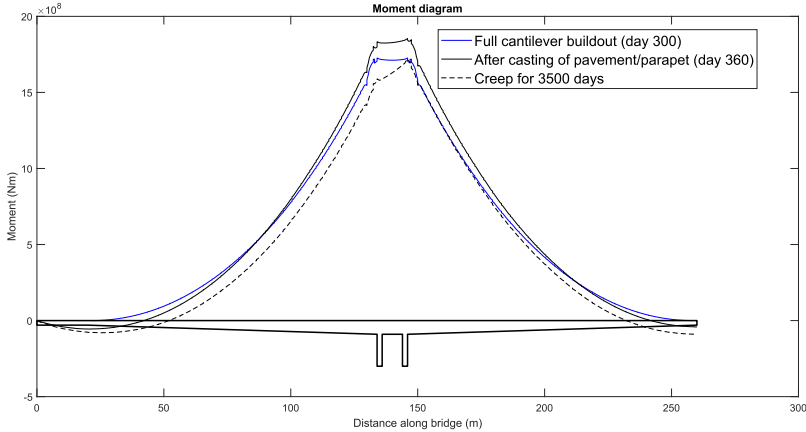


**Figure 7.10:** Bending moment when the tendons were neglected, at different time steps.

## 7.2.2 Influence of Tendons on the Bending Moment

The purpose of the post-tensioning tendons is to counteract the bending moment caused by the permanent loads applied to the bridge. This effect can be clearly seen in Figure 7.11, where the moment curve is shifted downwards when the final top tendons are tensioned. Note that the bending moment curves have been smoothed in MATLAB, which is the reason for the solid black line not being zero at the ends. Furthermore, Figure 7.12 shows how the effect of the tendons reduces with time. Note how the black dashed line moves towards the bending moment from when only permanent loads were considered.

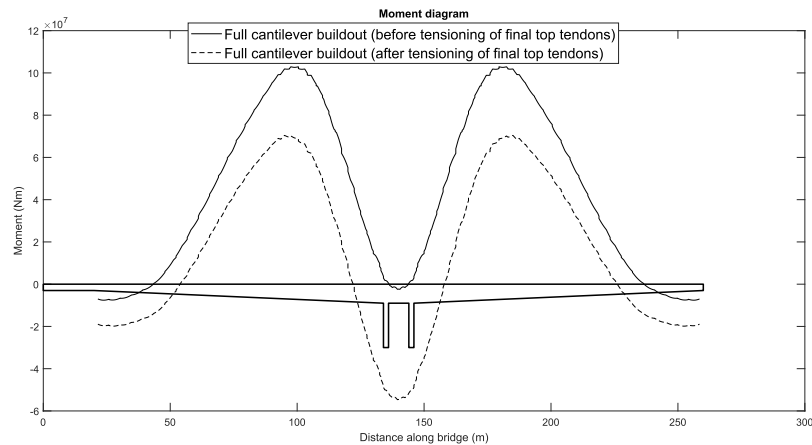


**Figure 7.11:** Effect of post-tensioning tendons, tensioning of final top tendons.

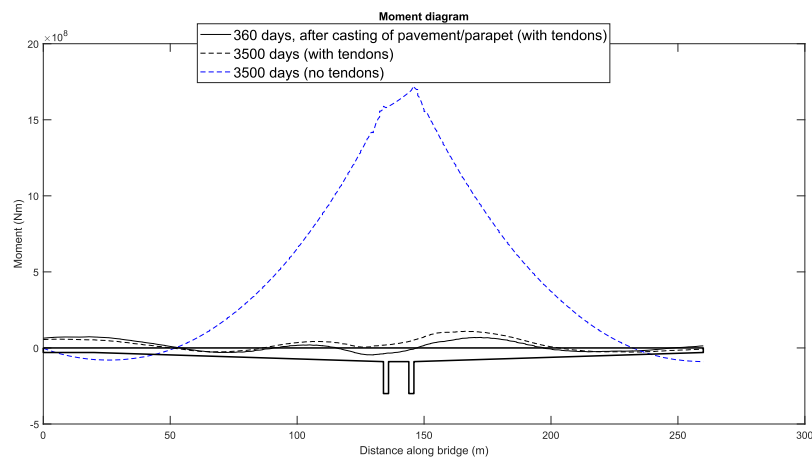


**Figure 7.12:** Creep effect for post-tensioning tendons.

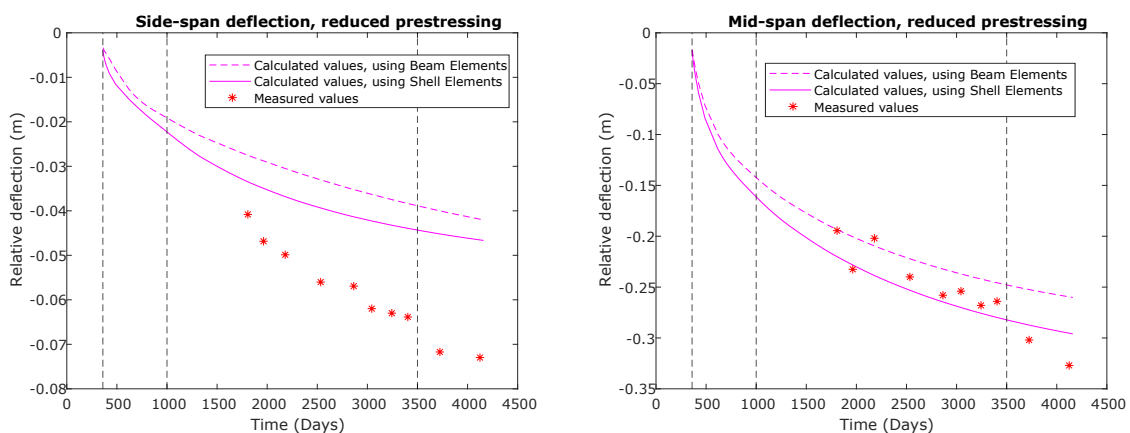
### 7.3 Calibration of Parameters

As shown in Huang et al. (2018), simply using the available models to predict creep deformations provide a poor estimation of the deflection history. The solution, according to Huang et al. (2018), is to add and calibrate coefficients for the creep, shrinkage, and prestress models. In this report the prestressing force will be reduced to see whether the deflections can be predicted more accurately. For many cases this has shown to be the determining factor, one example is the Koror-Babeldaob Bridge in Palau, where the prestress losses were measured to be around around 50 % over a period of 19 years (Bažant and Yu, 2013).

According to Bažant and Yu (2013), the prestressing losses needs to be calculated as part of a creep structural analysis (as done for this case study). It is also suggested that for creep sensitive structures, like large span segmentally built box girders, the losses in the tendons will be affected by temperature variations and strain in concrete (which is neglected in the current standard). The article proposes a constitutive relation for predicting the relaxation of prestressing steel, especially relevant for bridges with spans exceeding 80 meters. For example, at high temperatures ( $40^{\circ}C$ ), the relation given by Bažant and Yu (2013) predicts a steel relaxation of about 13 % after 4 years. The steel relaxation factor,  $\chi_{1000}$ , as a comparison, is only described for a constant temperature of  $20^{\circ}C$  and gave a final prestressing loss of 1.8 %. With the mean temperature in Chongqing being  $23^{\circ}C$  and much higher during the summer months (CustomWeather, 2021), as well as solar radiation increasing the daily temperature variation, a reasonable assumption is therefore that the prestressing losses of the Jiang Jin Bridge needs to be increased. To study this effect, a simplified logarithmic loss in stress due to steel relaxation is assumed, as described in equation 7.1. A similar relation is also used in the parametric study from Huang et al. (2018)). Using this relation, the losses due to steel relaxation reached about 20 % after 30 years. It is noticeable that the calibration provided a significantly better prediction of the real deflections (see Figure 7.13).

$$\sigma_p(t) = \sigma_{pi}(1 - 0.05\log_{10}(t)) \tag{7.1}$$

where  $\sigma_{pi}$  is the initial tension applied to the tendons and t is the elapsed time in days (from when the specific tendon was tensioned).



(a) Side-span deflections

(b) Mid-span deflections

**Figure 7.13:** Comparing deflections at mid- and side-span locations when the steel relaxation in the prestressed tendons were modified.

## 7.4 Sources of Errors

Regarding the collected data from Huang et al. (2018), a couple of assumptions made in the modelling need to be addressed:

- The cross section was simplified as an I beam with rectangular flanges and web, which leads to a slight error in the moment of inertia.
- The friction losses for the top tendons were neglected. In reality the top tendons might be slightly curved in the transversal direction, and friction losses would need to be taken into account.
- The measured deflections were described as "relative elevation surveys placed on the pavement after the Jiang Jin Bridge opened to traffic". The exact location of the side-span as well as the exact time of installation were not known. In this analysis the measurements were assumed to start after the pavement/parapet was added. If the relative measurements were to be initiated 10 days later in the model, the mid-span deflection would be reduced by 1.3 cm.

Regarding boundary conditions and loads the following should be considered:

- If the pylons were to be modelled as pinned, instead of rigid at the foundations, the results would be slightly different. The angular displacement at the top of the pylons would be reduced, which leads to an increase in deflection for the side-span and a decrease for the mid-span (see Figure 7.14). This way of modelling could possibly be more correct and could explain the discrepancy between the relative deflections for mid- and side-span.
- The weight of the superstructure (pavement/parapet) had to be estimated to 2.5 kPa. Large changes to this load could have significant effects on the time-dependant deformations.
- The fact that the weight of the travelling formwork was neglected should not affect the relative measurements much.

For the implementation of time-dependant losses in Abaqus, the following should be considered:

- The viscoelastic creep model had different input values depending on the notional size of the element. With varying thicknesses in the cross section of the concrete girder, as well as along the longitudinal length of the bridge, large simplifications had to be made. Modelling with shell elements allowed for the most exact implementation.
- For the shrinkage, an average notional size was assumed for the whole bridge girder. This should not affect the long-term deformations much since the notional size mostly influences the rate of the shrinkage. The creep of concrete and losses in prestressing tendons have also shown larger impact during the modelling of the case study.
- As a simplification in the modelling, the concrete segment instantly started to carry its own weight. When considering the long-term effects, however, the error due to this simplification is considered to be quite small.

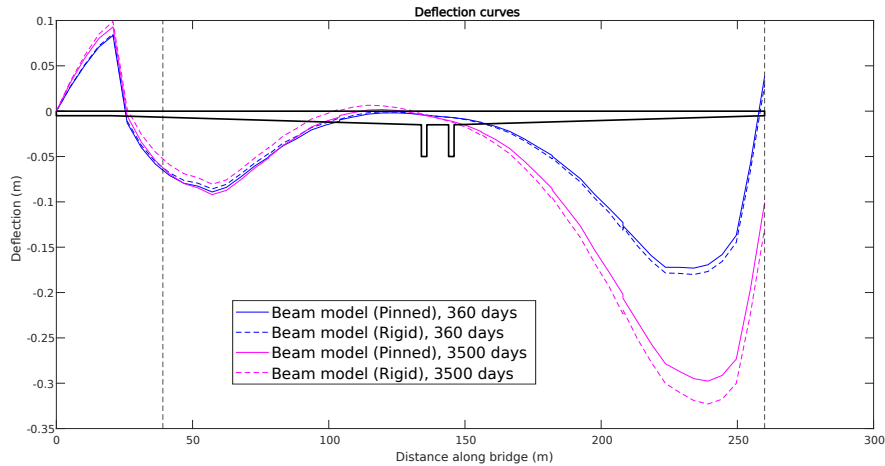


**Figure 7.14:** Deflection curves obtained from Abaqus at different times. Showing the difference when the foundations are modelled as pinned instead of rigid.

Regarding the accuracy of the viscoelastic creep model it was shown, in section 4.3, to capture the behaviour described in EC. This behaviour is, however, a simplification. There are other, more advanced models that have shown to capture the long-term behaviour more accurate, for example model B3 and the recently updated model B4. Using these models could improve the results slightly but would not be enough to explain the excessive deflections. As shown in the report by Huang et al. (2018), the mid-span deflection of the Jiang Jin Bridge could not be predicted by using model B3.

Some structural deficiencies were detected from a bridge survey which, most likely, increased the long-term deformations (Huang et al., 2018):

- Inclined cracks were discovered on the web, approximately 40 meters from the mid-span. Bending cracks were also observed within 3 meters from the mid-span.
- It was discovered that a wedge was missing from one tendon and voids were detected in the grouting.

As described in section 3.2.3, the creep calculations are based on the compressive stresses being below  $0.45f_{ck}$ . Figure 7.15 shows that this value is exceeded locally in a couple of elements. For the long-term behaviour, however, this is assumed to have a neglectable effect.

As can be seen for both the shell and beam model, the pylons stopped at the bottom flange of the concrete girder. In reality, there are large compressive forces that needs to be distributed to the foundation, and there would have to be stiffeners in the girder above the pylons. These stiffeners are, however, not modelled in this case study (which is one reason for the large principal stresses by the support shown in Figure 7.15). This also causes the models to be slightly softer, resulting in larger deflections. By modelling stiffeners and analysing the difference regarding the long-term behaviour, it is concluded that this error is neglectable for the purpose of this analysis.

When calculating the losses in the tendons due to steel relaxation in EC, the relaxation factor after 1000 hours,  $\chi_{1000}$ , is based the initial force in the tendons being 70 % of the actual tensile strength. However, in the manufacture brochure *European Technical Approval ETA-08/0012*



Principal stress (MPa)

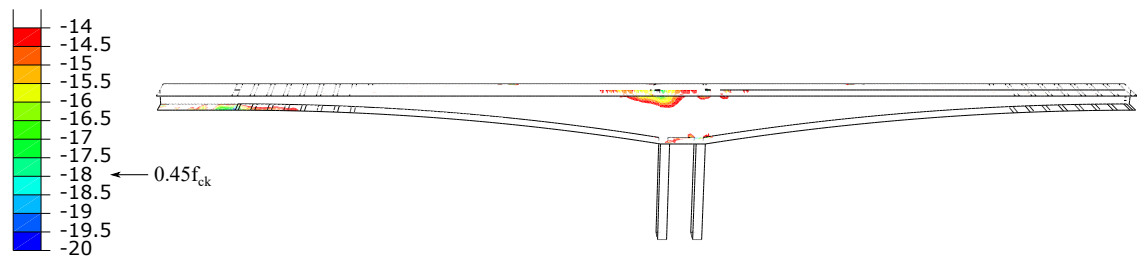


**Figure 7.15:** Areas where the principle stress is close to  $0.45f_{ck}$ , which is the limit for the calculations regarding the creep factor,  $\varphi(t, t_0)$ .

*Tensacciai Post-Tensioning Systems* (2017), the initial force is compared to the characteristic tensile strength, which gives a utilization degree of 75 % in the case study (see section 6.3.1). In the updated version of Eurocode 2 (2018), and in the manufacturing brochure *European Technical Approval ETA-08/0012 Tensacciai Post-Tensioning Systems* (2017),  $\chi_{1000}$  is also given for tendons with an initial force of 80 % of its actual and characteristic tensile strength. The value of  $\chi_{1000}$  for relaxation class 2 can then be read as 0.045, instead of 0.025. If 0.045 is chosen, the total loss due to steel relaxation would be 3.24 %, 1.8 times higher than the calculated losses in this report. The measured deflections would, however, still not be achieved.



# 8 Conclusions

The overarching objective of the present work was to model time-dependent losses in segmentally constructed concrete bridges, with special emphasis on the effect of creep. This was done by establishing a routine for numerical modelling. The main conclusions of the subsequent analysis are summarized as follows:

1. The effect of early and repeated loading is difficult to predict. Numerical simulation of a simple load case indicated that a viscoelastic model, based on the creep function in EC, was the most accurate. This conclusion is corroborated by similar studies in the literature, which strengthens the results.
2. Through modelling of the Jiang Jin Bridge, it was shown that the viscoelastic model can be useful for modelling creep in more complex structures, specifically segmentally constructed bridges. Discrepancy between measured results were however observed, leading to the conclusion that other factors need to be considered.
3. The discrepancies described in the previous point could be partly eliminated through significantly increasing the time-dependent losses of the prestressing tendons. This points towards time-dependent losses being underestimated. This is not surprising since measurements have shown large reductions in prestressing force for similar structures, largely due to high temperature variations. To accurately predict the deflections these losses would need to be more accurately studied and implemented along with the creep model.
4. Modelling with beam elements significantly reduces modelling and computational time, as well as the file size of the actual model. Using shell elements, however, allowed for a more accurate implementation of the viscoelastic creep model and captured the long-term behaviour better.
5. The viscoelastic creep model can be easily applied to all concrete structures and depends solely on the creep function from EC. A conclusion can be drawn that the model is able to capture the behaviour from EC very well. It should be noted that the accuracy of the creep model is limited to the behaviour according to the General and incremental step-by-step method (see section 4.1). To assess the accuracy of the creep model, the General and incremental step-by-step method needs to be studied in detail.



## 9 Further Work

The subject studied in this Master's Thesis is quite extensive, only a specific part was thoroughly investigated. This leads to further work being required, to reliably predict long-term deformations for segmentally constructed prestressed concrete bridges. Here follows a couple of suggestions:

- This report studies one way of implementing the viscoelastic model in Abaqus. It would be of interest to investigate other ways, possibly increasing the accuracy and reducing the modelling time.
- Due to a limited amount of data for the case study, some simplifications and assumptions have been made. It would be of interest to perform a similar analysis in a case-study where the full and accurate history of the bridge is known.
- For the Jiang Jin Bridge the deflection history was measured over a period of 10 years. It would be of interest to perform the analysis when deflections over a larger period are available. Continuous measurements of losses in prestressed tendons would also allow for a better analysis.
- Shrinkage and prestress losses were in this report implemented using amplitude functions (tabular). It would be of interest to investigate the best and easiest way of implementing these in Abaqus.
- The viscoelastic creep model predicted larger deformations when shell elements were used, compared to beam elements. Further analysis is required, however, to determine and isolate the accuracy of the creep model with respect to shell and beam elements.
- It would be of interest to perform the analysis using solid elements, which has not been done in this report.



# Bibliography

## Articles

- Allos, Atheel E and LH Martin (1981). ‘Factors affecting Poisson’s ratio for concrete’. In: *Building and environment* 16.1, pp. 1–9.
- Bazant, Zdeněk P, Qiang Yu and Guang-Hua Li (2012a). ‘Excessive long-time deflections of prestressed box girders. I: Record-span bridge in Palau and other paradigms’. In: *Journal of structural engineering* 138.6, pp. 676–686.
- (2012b). ‘Excessive long-time deflections of prestressed box girders. II: Numerical analysis and lessons learned’. In: *Journal of Structural Engineering* 138.6, pp. 687–696.
- Bažant, Zdeněk P and Qiang Yu (2013). ‘Relaxation of prestressing steel at varying strain and temperature: Viscoplastic constitutive relation’. In: *Journal of Engineering Mechanics* 139.7, pp. 814–823.
- Billington, Philip N, David P Billington and Hubert. Shirley-Smith (2020). ‘Bridge’. In: *Encyclopedia Britannica*. URL: <https://www.britannica.com/technology/bridge-engineering>.
- Dai, Gonglian, Hao Ge, Miao Su and Y Frank Chen (2017). ‘Century-old covered bridge with cantilever beams in China’. In: *Structural Engineering International* 27.2, pp. 255–262.
- Grasley, Zachary C and David A Lange (2007). ‘What is balanced Cantilever method of Bridge Construction?’ In: *Mechanics of Time-Dependent Materials* 11.3-4, pp. 175–198.
- Huang, Haidong, Shan-Shan Huang and Kypros Pilakoutas (2018). ‘Modeling for assessment of long-term behavior of prestressed concrete box-girder bridges’. In: *Journal of Bridge Engineering* 23.3, p. 04018002.
- Kwak, H.-G. and J.-K. Son (2002). ‘Determination of design moments in bridges constructed by balanced cantilever method’. In: *Engineering Structures* 24.5, pp. 639–648. ISSN: 0141-0296.
- Loewe, Sanabra and Capellà Llovera (2014). ‘The four ages of early prestressed concrete structures’. In: *PCI Journal* 59.4, pp. 93–121.
- Lucko, Gunnar and Jesús M de la Garza (2003). ‘Constructability considerations for balanced cantilever construction’. In: *Practice Periodical on Structural Design and Construction* 8.1, pp. 47–56.
- Mistewicz, Marek (2015). ‘First European truss cantilever bridge in the light of numismatics, iconography and written sources’. In: *Kwartalnik Architektury i Urbanistyki*.
- Reiner, M (1949). ‘On volume-or isotropic flow as exemplified in the creep of concrete’. In: *Flow, Turbulence and Combustion* 1.1, p. 475.

## Book Sources

- Ashter, Syed Ali (2018). *Thermoforming of Single and Multilayer Laminates*. Taylor, Francis.
- Betten, Josef (2008). *Creep mechanics*. Springer Science & Business Media.
- Council, National Research et al. (1997). *Nonconventional concrete technologies: renewal of the highway infrastructure*. Vol. 484. National Academies Press.
- Engström, Björn (2008). *Restraint cracking of reinforced concrete structures*. Chalmers University of Technology.
- Hendy, Chris R. and David A. Smith (2007). *Designers' Guide to EN 1992-2 Eurocode 2: Design of concrete structures: Part 2: Concrete bridges*. The authors and Thomas Telford Limited 2007.
- Nguyen, Ngoc-Vinh, Quoc-Anh Vu and Seung-Eock Kim (2020). *Construction and Building Materials*. Elsevier.

## Manuals

- ASTM International (2018). *Standard Specification for Low-Relaxation, Seven-Wire Steel Strand for Prestressed Concrete*. ASTM International.
- Eurocode 2 (2005a). *SS-EN 1992-1-1, Eurocode 2: Design of concrete structures – Part 1-1: General rules and rules for buildings*. SIS AB.
- (2005b). *SS-EN 1992-2, Eurocode 2 – Design of concrete structures – Part 2: Concrete bridges – Design and detailing rules*. SIS AB.
- (2018). *SS-EN 1992-1-1, Eurocode 2 – Design of concrete structures (Updated version) – Part 1-1: General rules and rules for buildings*. SIS AB.
- Simulia (2014). *ABAQUS 6.14 - ANALYSIS USER'S GUIDE VOLUME III: MATERIALS*. Dassault Systemes.

## Websites

- CustomWeather (2021). *Annual Weather Averages Near Chongqing*. URL: <https://www.timeanddate.com/weather/china/chongqing/climate> (visited on 05/05/2021).
- Ohlsson, Gabriel (2018). *What is a Viscoelastic material?* URL: <https://www.biolinscientific.com/blog/what-is-a-viscoelastic-material> (visited on 18/02/2021).

## Reports

- Engström, Björn (2011). *Design and analysis of prestressed concrete structures*. Report. CHALMERS UNIVERSITY OF TECHNOLOGY.
- European Technical Approval ETA-08/0012 Tensacciai Post-Tensioning Systems* (2017). Brochure.



## Theses

Canovic, Senad and Joakim Goncalves (2005). ‘Modelling of the response of the New Svinesund Bridge’. Master’s Thesis. CHALMERS UNIVERSITY OF TECHNOLOGY.

Teng, Tong (2017). ‘Computational Modelling of Concrete Time-Dependent Mechanics and Its Application to Large-Scale Structure Analysis’. University of Pittsburgh.